High-*P* behavior of anorthite composition and some phase relations of the CaO-Al_2O_3-SiO_2 system to the lower mantle of the Earth, and their geophysical implications

Xi Liu,[1,2] Hiroaki Ohfuji,[1] Norimasa Nishiyama,[1] Qiang He,[2] Takeshi Sanehira,[1] and Tetsuo Irifune[1]

Received 6 March 2012; revised 22 July 2012; accepted 8 August 2012; published 20 September 2012.

[1] Multianvil experiments with long experimental durations have been made with the anorthite composition $CaAl_2Si_2O_8$ at pressure-temperature (*P-T*) conditions of 14–25 GPa and 1400–2400°C. At subsolidus conditions, these experiments demonstrated three phase assemblages, grossular (Gr) + kyanite (Ky) + stishovite (St) at ~14 GPa, Gr + calcium-alumino-silicate phase (CAS) + St at ~18 GPa, and CAS + $CaSiO_3$-perovskite (CaPv) + St at above ~20 GPa, which are related by the reactions Gr + Ky = CAS + St and Gr + St = CAS + CaPv. Following the method of Schreinemakers, we combined our data with the literature data to deduce a *P-T* phase diagram for a portion of the CaO-Al_2O_3-SiO_2 system at subsolidus conditions, which subsequently helped to solve some long-lasting discrepancies in the high-*P* behavior of the compositions of anorthite and grossular. The crystal chemistry of the CAS and CaPv solid solutions was examined, and new substitution mechanisms were firmly established. Along the solidus, the melting reaction at ~14 GPa is peritectic while that at ~22 GPa is eutectic. For both pressures, St is the first phase to melt out and the melt is generally andesitic. For the An composition, its density starts to be significantly higher than the density of pyrolite at ~2.5 GPa, a much lower pressure than that for the Or, Ab or Qtz composition (~7.5–10 GPa), so that the An-enriched continental crust material should readily plunge into the upper mantle.

Citation: Liu, X., H. Ohfuji, N. Nishiyama, Q. He, T. Sanehira, and T. Irifune (2012), High-*P* behavior of anorthite composition and some phase relations of the CaO-Al_2O_3-SiO_2 system to the lower mantle of the Earth, and their geophysical implications, *J. Geophys. Res.*, *117*, B09205, doi:10.1029/2012JB009290.

1. Introduction

[2] According to the composition models proposed by *Taylor and McLennan* [1985] and *Rudnick and Fountain* [1995], the continental crust is mainly made of feldspar (>60%, with the proportions of the three end-members orthoclase (Or), albite (Ab) and anorthite (An) being 11.1%, 27.1% and 23.2%, respectively), quartz (~15%; Qtz; SiO_2) and pyroxene (~15%). During the subduction process along the oceanic trench, the continental crust material might be brought down to the deep interior of the Earth, then physically and chemically interact with the mantle material, and eventually affect the geodynamic process of the Earth [*Dupré and Allègre*, 1983; *Irifune et al.*, 1994; *Hofmann*, 1997; *Wu et al.*, 2009]. To understand this process, it is therefore important to investigate the high pressure (*P*) behavior of the constituent phases of the continental crust material. Due to the geological significance and chemical simplicity of Qtz, its phase transitions at high pressures have been extensively studied and well established: at pressures lower than approximately 9 GPa, first Qtz and then coesite (Coe) are the stable forms of SiO_2, and both phases are more buoyant than the peridotitic upper mantle material [*Angel et al.*, 2001]; at higher pressures, stishovite (St) comes to be stable and it is substantially more dense than peridotite [*Andrault et al.*, 2003]. The more significant constituent phase of feldspar also has been widely investigated, but its high-*P* behavior has been much less well established so far, mainly due to its chemical complexity. Following the composition model proposed by *Rudnick and Fountain* [1995], the average composition of feldspar in the continental crust is approximately 18.1% Or, 44.1% Ab and 37.8% An.

[3] Many high-*P* studies with different methods have been conducted to disclose the high-*P* behavior of feldspar [e.g., *Ringwood et al.*, 1967; *Liu*, 1978; *Yagi et al.*, 1994; *Gautron et al.*, 1996; *Akaogi et al.*, 2004a; *Sueda et al.*, 2004; *Nishiyama et al.*, 2005; *Liu*, 2006; *Hirao et al.*, 2008;

[1]Geodynamics Research Center, Ehime University, Matsuyama, Japan.
[2]Ministry of Education Key Laboratory of Orogenic Belts and Crustal Evolution, School of Earth and Space Sciences, Peking University, Beijing, China.

Corresponding author: X. Liu, Ministry of Education Key Laboratory of Orogenic Belts and Crustal Evolution, School of Earth and Space Sciences, Peking University, Beijing 100871, China. (xi.liu@pku.edu.cn)

0148-0227/12/2012JB009290

Mookherjee and Steinle-Neumann, 2009; *Deng et al.*, 2010, 2011], and significant progress has been achieved. As summarized in *Liu et al.* [2010a], Ab ($NaAlSi_3O_8$) breaks down to jadeite (Jd; $NaAlSi_2O_6$) + Qtz at ~2.5 GPa [*Birch and LeComte*, 1960; *Liu*, 1978; *Holland*, 1980], which in turn transforms into Jd + Coe at ~3 GPa, then into Jd + St at ~9 GPa and finally into calcium ferrite-structured $NaAlSiO_4$ (CF) + St at ~22 GPa [*Liu*, 1978; *Yagi et al.*, 1994; *Tutti et al.*, 2000; *Deng et al.*, 2010]. The average density of the isochemical phase assemblages Ab, Jd + Qtz and Jd + Coe is significantly lower than, that of the phase assemblage Jd + St generally higher than, and that of the phase assemblage CF + 2St broadly identical to, that of the surrounding mantle material (pyrolite) [*Ringwood*, 1966]. On the other hand, Or ($KAlSi_3O_8$) is stable with the structure of sanidine (San) at low pressures and decomposes into wadeite-structured $K_2Si_4O_9$ (Wd) + kyanite (Ky) + Coe at ~6 GPa [*Kinomura et al.*, 1975; *Liu*, 1987; *Urakawa et al.*, 1994; *Yagi et al.*, 1994], which subsequently transforms into Wd + Ky + St at ~9 GPa. At approximately 10 GPa, these three phases, Wd, Ky and St, recombine to form a hollandite-type phase with the composition of $KAlSi_3O_8$ (Holl-I). At ~23 GPa, the structure of Holl-I is deformed and an isochemical new phase forms (Holl-II) [*Sueda et al.*, 2004; *Nishiyama et al.*, 2005; *Ferroir et al.*, 2006; *Deng et al.*, 2011]. Compared to the density of the mantle material at similar pressures, the density of the isochemical phase assemblages of San and Wd + Ky + Coe is generally low, that of the phase assemblages of Wd + Ky + St and Holl-I relatively high, and that of Holl-II broadly similar. If the materials of Ab and Or are subducted down to about 9 GPa, they will enter the deep interior of the Earth rather than positively return to the shallow depths. Eventually, they will be trapped at around the upper mantle-low mantle boundary because they become buoyant there.

[4] In the case of the third end-member of feldspar, An ($CaAl_2Si_2O_8$), our current knowledge is in pieces, in controversy and incomplete. As summarized by *Liu et al.* [2010a], early high-*P* experimental work demonstrated the consecutive subsolidus phase assemblage sequence An → grossular (Gr) + Ky + Qtz → Gr + Ky + Coe → Gr + Ky + St up to about 10 GPa [*Boyd and England*, 1961; *Reid and Ringwood*, 1969; *Goldsmith*, 1980] while more recent work observed the phase assemblage Gr + CAS (a calcium-alumino-silicate phase first observed by *Irifune et al.* [1994]) +St at about 14 GPa [*Gautron et al.*, 1996]. Because of the ~4 GPa pressure gap, it is not clear if the phase assemblages of Gr + Ky + St and Gr + CAS + St are directly related to each other. *Gautron and Madon* [1994] carried out some laser heated diamond-anvil cell (DAC) experiments up to ~22.5 GPa, and observed a phase assemblage of hollandite-type $Ca_{1.33}Al_{1.33}Si_{2.33}O_8$ + Ky-type Al_2SiO_5 + calcium perovskite-type $Ca_{0.8}Al_{0.4}Si_{0.2}O_3$ (CaPv) at around 14 GPa, which is hard to reconcile with other experimental results [*Liu*, 1974; *Irifune et al.*, 1995; *Gautron et al.*, 1996]. With the unavailability of a complete *P-T* phase diagram for the An composition, much is unknown about the geophysical behavior of the An composition at high pressures.

[5] This study has been designed to experimentally investigate the equilibrium phase relations of the An composition up to the uppermost lower mantle of the Earth, hoping that we could fill up the ~4 GPa pressure gap, clarify the phase relations at ~14 GPa, explore the *P-T* diagram at higher pressures. With the new experimental data, the geophysical consequences resulting from the high-*P* phase transitions of the An composition will be discussed.

2. Experimental Details

[6] High-purity chemicals SiO_2, Al_2O_3 and $CaCO_3$ were used to prepare the starting material for the high-*P* experiments. First, these chemicals were heated at 450°C and one atm for 24 h to remove any possible water. Second, the dried chemicals were weighed, thoroughly mixed and ground under acetone in an agate mortar, and subsequently pelletized. Third, the resulting material was heated at 1050°C and 1 atm for 24 h to remove CO_2, then melted at 1650°C and 1 atm for 20 min [*Presnall*, 1995], and quenched into a clear and homogeneous glass, as revealed by later examinations with an optical microscope and an electron microprobe in an EDS mode. Eventually this glass was ground, and then stored in an oven at 110°C and room *P* for later high-*P* experiments.

[7] The high-*P* experimental techniques and characterizing methods in the present investigation were identical to those reported in *Liu* [2006], so that they are only briefly mentioned here.

[8] Our high-*P* experiments were conducted by using a 2000-ton double stage multianvil (MA) press installed at the Geodynamics Research Center of Ehime University. Tungsten carbide cubes with 3.0 mm truncated edge length, separated and supported by pyrophilite gaskets, were used as the second stage anvils. Co-doped MgO blocks were used to prepare the pressure medium, which had its shape identical to but its size (3.0 rather than 2.0 mm) different to that shown in *Nishiyama and Yagi* [2003, Figure 2]. The *P* calibration was based on the electrical resistance changes associated with the phase transitions of ZnS, GaAs and GaP at ambient *T*, and its uncertainty was ~0.5 GPa. For certain oil pressure, however, the experimental pressures at high *T* and ambient *T* can be different due to the trade-off between material relaxation and thermal pressure; according to *Ito and Takahashi* [1989], *Fei and Bertka* [1999], and *Nishiyama and Yagi* [2003], the uncertainty of our *P* measurement at high *T* could be less than ±1 GPa. *T* was measured by using a $W_{97}Re_3$-$W_{75}Re_{25}$ thermocouple, with the assumption of a negligible effect of *P* on its e.m.f. The uncertainty in the *T* measurement might be in the order of 50 degrees. The basic experimental cell arrangement was similar to that described in *Nishiyama and Yagi* [2003], with the exceptions of different cell sizes and different capsule materials. The initial length of the cylindrical Pt or Re capsules (OD = 0.8 mm and ID = 0.6 mm for the Pt capsules; OD = 0.7 mm and ID = 0.5 mm for the Re capsules) before the high-*P* experiments was about 1.0 mm, which might lead to a temperature gradient of about 100°C in the experimental charges [*Bertka and Fei*, 1997]. In all high-*P* experiments, the present starting material was simultaneously run with another material of the $(K_{0.2}Na_{0.8})AlSi_3O_8$ composition; the experimental results for the latter material were already reported in *Liu* [2006].

[9] For the experiments which generated large phase grains, we mainly relied on an SEM in EDS mode to identify

Table 1. Experimental Conditions and Results[a]

Run Number	*P*	*T*	*t*	Phases Observed	Note
OS-1245	14	1400	26	Gr, Ky, St	Fine grained
OS-1253[b]	14	1600	12	Gr, Ky, St	
OS-1247	14	1800	7.5	Gr, Ky, St, Melt	
OS-1278	14	2000	1	Gr, Ky, Melt	Low-*T* end
				Cor, Ky, Melt	High-*T* end
OS-1258	18	1600	12	Gr, CAS, St	Fine grained
OS-1261	18	1800	6	Gr, CAS, St	
OS-1264	18	2000	4	Gr, CAS, St	
OS-1279[c]	18	2200	1.7	Gr, CAS, St	Fine grained
OS-1266	22	1600	29.4	CAS, CaPv, St	Fine grained
OS-1262	22	1800	6.1	CAS, CaPv, St	
OS-1272	22	2000	5.3	CAS, CaPv, St	
OS-1378[c]	22	2200	2	CAS, CaPv, St	Fine grained
OS-1376[c]	22	2400	0.2	CAS, CaPv, Melt	
OS-1274	25	1400	30	CAS, CaPv, St	Fine grained
OS-1268	25	1600	41	CAS, CaPv, St	Fine grained
OS-1263	25	1800	8	CAS, CaPv, St	Fine grained
OS-1269	25	2000	4	CAS, CaPv, St	

[a]*P*, pressure in GPa; *T*, temperature in °C; *t*, time in hours.
[b]Temperature controlled by input electrical power due to thermocouple failure.
[c]Rhenium capsule rather than platinum capsule used.

and compositionally characterize the phases. The working conditions of the SEM were 15 kV, 0.885 nA, <1 μm beam spot and collecting time of 50 s per analysis. The accuracy of the EDS analysis was demonstrated by 11 replicate analyses of the homogeneous starting material of the An composition, performed during different analytical sessions: SiO_2 43.88(17), Al_2O_3 36.62(25) and CaO 19.24(20) in weight. For the experiments which generated very fine grains, we also used a micro-focus X-ray diffractometer (M18XHF) to facilitate identifying the phases. To check if there was any experimental contamination, we routinely analyzed for the concentrations of TiO_2, Cr_2O_3, MgO, FeO, MnO, Na_2O and K_2O in all the presenting phases. With the exception of one experiment (OS-1278; some MgO contamination), all other experiments were found to be contamination-free. Water contents in the experiments were not checked, but they are believed to be negligible (more discussion later).

3. Phase Relations and Phase Compositions

[10] We conducted 17 MA experiments: 14 subsolidus experiments and 3 supersolidus experiments. The conditions and results of the experiments are summarized in Table 1, and some observed phase compositions are listed in Table 2.

[11] Figure 1 shows some typical BSE images for the experimental products. Although the *P-T-t* (time) conditions for the experiments with the An composition were identical to those for the experiments with the $Or_{20}Ab_{80}$ composition [*Liu*, 2006], the experimental products looked rather different. In the experiments with the $Or_{20}Ab_{80}$ composition, large and homogeneous crystals were always successfully synthesized. In contrast, the experiments with the An composition frequently resulted in fine-grained phases (Table 1).

Table 2. Compositions of Some Observed Phases[a]

Run Number	*T* (°C)	Phase	SiO_2	Al_2O_3	MgO	CaO	Si	Al	Mg	Ca	Total	Note
						14 GPa						
OS-1253	1600	Gr(16)[b]	40.34(59)[c]	24.07(82)	-	35.60(64)	3.00(4)	2.11(7)	-	2.84(6)	7.95(2)	
		Ky(11)	37.30(35)	62.45(36)	-	0.24(15)	1.01(1)	1.99(1)	-	0.01(1)	3.00(1)	
OS-1247	1800	Gr(10)	40.88(27)	23.15(23)	-	35.97(40)	3.04(2)	2.03(1)	-	2.87(4)	7.94(2)	
		Ky(6)	36.93(16)	62.99(21)	-	0.08(13)	1.00(1)	2.00(1)	-	0.00(1)	3.00(1)	
OS-1278	2000	Gr(7)	40.66(16)	23.08(33)	1.80(72)	34.47(90)	3.02(1)	2.02(2)	0.20(8)	2.74(8)	7.97(1)	Low-*T* end
		Ky(4)	36.98(22)	62.58(23)	0.34(6)	0.09(8)	1.00(0)	1.99(1)	0.01(1)	0.00(1)	3.00(1)	Low-*T* end
		Gr(3)	41.11(24)	23.10(13)	3.38(106)	32.42(122)	3.03(1)	2.01(2)	0.37(11)	2.56(11)	7.96(1)	Middle part
		Cor(5)	2.34(9)	96.56(14)	1.14(5)	0.00(0)	0.04(0)	1.93(0)	0.03(0)	0.00(0)	2.00(0)	High-*T* end
		Ky(5)	37.24(27)	62.28(25)	0.39(7)	0.09(8)	1.00(1)	1.98(1)	0.02(1)	0.00(0)	3.01(1)	High-*T* end
		Melt(13)	55.51(57)	20.01(233)	2.63(19)	21.84(210)						High-*T* end
						18 GPa						
OS-1261	1800	Gr(12)	41.35(34)	23.21(30)	-	35.44(57)	3.07(2)	2.03(2)	-	2.82(5)	7.92(2)	
		CAS(11)	33.86(82)	51.98(99)	-	14.17(46)	2.13(5)	3.86(8)	-	0.96(3)	6.94(2)	
OS-1264	2000	Gr(15)	41.28(44)	22.94(47)	-	35.77(63)	3.06(2)	2.01(4)	-	2.84(6)	7.91(3)	
		CAS(14)	33.69(94)	52.20(102)	-	14.11(78)	2.12(5)	3.87(8)	-	0.95(6)	6.94(3)	
						22 GPa						
OS-1262	1800	CAS(12)	33.17(75)	52.33(64)	-	14.50(71)	2.09(4)	3.89(5)	-	0.98(5)	6.96(3)	
OS-1272	2000	CAS(11)	32.07(29)	53.19(15)	-	14.74(24)	2.03(1)	3.96(1)	-	1.00(2)	6.99(2)	
OS-1376	2400	CAS(8)	32.65(37)	52.82(60)	-	14.53(42)						
		Melt(12)	64.04(40)	15.80(37)	-	20.15(21)						
						25 GPa						
OS-1263	1800	CAS(11)	35.39(190)	50.06(150)	-	14.55(54)	2.22(11)	3.70(12)	-	0.98(4)	6.90(5)	
OS-1269	2000	CAS(14)	33.97(137)	51.58(115)	-	14.45(61)	2.13(8)	3.81(10)	-	0.97(4)	6.92(4)	Low-*T* end
		CAS(7)	33.39(93)	51.94(117)	-	14.67(48)	2.10(6)	3.84(9)	-	0.99(3)	6.93(3)	Middle part
		CAS(15)	32.63(52)	52.40(80)	-	14.97(50)	2.06(3)	3.89(6)	-	1.01(4)	6.96(2)	High-*T* end
		CAS(36)	33.51(144)	51.78(137)	-	14.71(57)	2.11(8)	3.83(11)	-	0.99(4)	6.93(4)	All data

[a]The abundance of the oxides is in weight unit and normalized to a total of 100%. The ion numbers are calculated on the basis of 5 oxygens for Ky, 12 oxygens for Gr, 3 oxygens for Cor, and 11 oxygens for CAS.
[b]The numbers in parentheses following the run number is the number of the electron microprobe analyses performed.
[c]40.34(59) should be read as 40.34 $\pm$ 0.59.

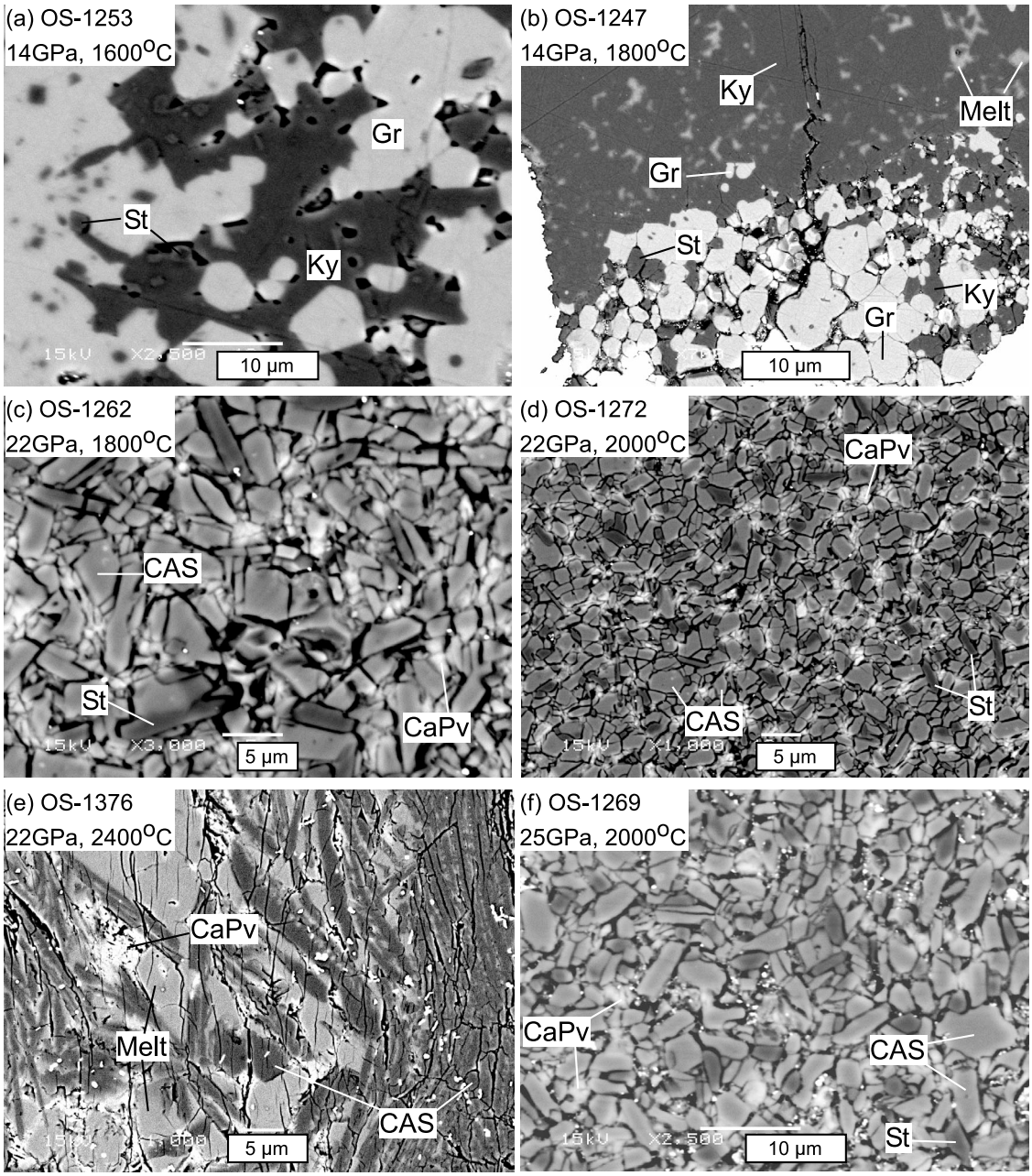

Figure 1. BSE images: (a) OS-1253 (14 GPa, 1600°C), (b) OS-1247 (14 GPa, 1800°C), (c) OS-1262 (22 GPa, 1800°C), (d) OS-1272 (22 GPa, 2000°C), and (e) OS-1376 (22 GPa, 2400°C), (f) OS-1269 (25 GPa, 2000°C). Ky, kyanite; Gr, grossular; St, stishovite; CAS, calcium-alumino-silicate phase with the general formula of $CaAl_4Si_2O_{11}$; CaPv, unquenchable Al-bearing calcium perovskite. Note the compositional layering in Figure 1b potentially caused by the Soret effect, with the hot end lacking in CaO. The melt in Figure 1b has a very low fraction, and did not quench to clear glass. The melt in Figure 1e shows extensive dendritic melting texture, and special morphology of the CAS phase, which is much comparable to the observation of *Keshav and Gudfinnsson* [2010].

This different high-*P* behavior partially reflects the refractory nature of the An composition, compared to the $Or_{20}Ab_{80}$ composition, and partially reflects the complexity of the subsolidus phase relations for the investigated *P* interval (more discussion later).

[12] For the experiments at ~14 GPa (from 1400 to 2000°C), we observed the subsolidus phase assemblage Gr + Ky + St, and the supersolidus phase assemblages Gr + Ky + St + Melt, Gr + Ky + Melt, and Cor (corundum) + Ky + Melt. Previously, the stability of the subsolidus phase assemblage Gr + Ky + St was experimentally demonstrated up to ~10 GPa [*Reid and Ringwood*, 1969]. Since *Gautron et al.* [1996] observed the subsolidus phase assemblage of Gr + CAS + St at ~14 GPa, it follows that the transition *P* between these two subsolidus phase assemblages must be close to 14 GPa. The melt in OS-1247 had a

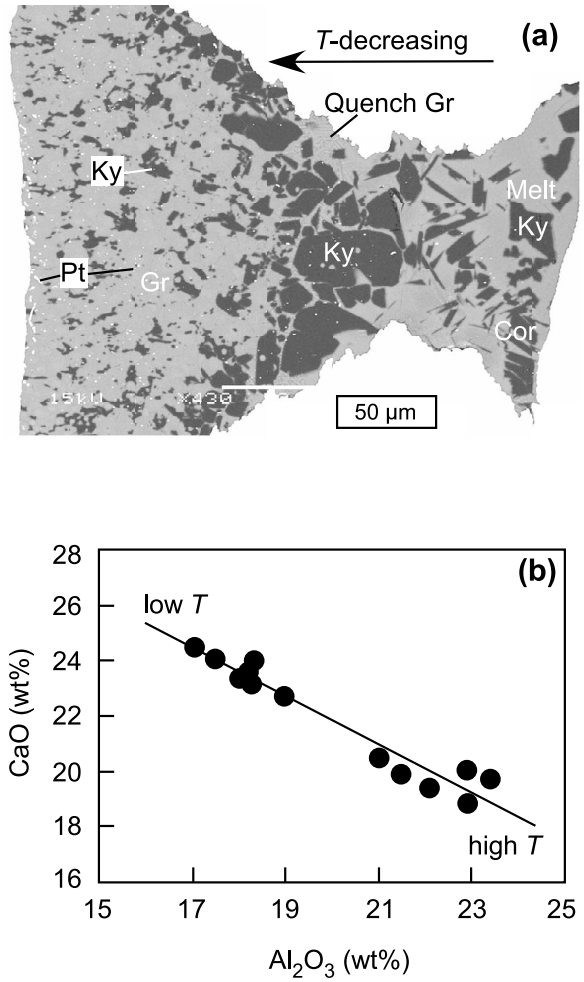

Figure 2. OS-1278 at 14 GPa and 2000°C: (a) BSE image of the entire charge and (b) variation of the contents of CaO and Al_2O_3 of the clear melts, showing potential Soret effect.

rather low proportion (Figure 1), and did not quench to clear glass, leading to large compositional variation (Table 2). On the other hand, the melt area at the high-*T* end of the experiment OS-1278 (Figure 2a), with the presence of Ky and Cor, is large and free of quench crystals; the large composition variation (Table 2), with systematically increasing Al_2O_3 content but decreasing CaO content from the low-*T* part to high-*T* part of the melt area (Figure 2b), might result from the Soret effect [*Lesher and Walker*, 1988]. At the low-*T* end of the capsule, the observed phase assemblage is Gr + Ky + Melt (trace). At the middle part of the capsule, numerous fine Gr quench crystals were observed to coexist with the equilibrium solid phases of Gr and Ky, suggesting that the melt was generally saturated with the Gr component. Additionally, OS-1278 was slightly contaminated by the MgO sleeve surrounding the Pt capsule, as revealed by the composition data (Table 2); the effect of this small amount of MgO on the phase relations is ignored in this study.

[13] The experiments at 18 GPa (from 1600 to 2200°C) generated a subsolidus phase assemblage Gr + CAS + St only, suggesting that this phase assemblage has a rather high solidus *T*. The refractory nature of this phase assemblage is also indicated by the small grain sizes of the phases, which usually prevented collecting compositional data with high quality. Especially, the small grain size in OS-1279 at 2200°C is rather interesting, considering the very high experimental *T* and long run duration (Table 1). A close *P-T* location of this experiment to one subsolidus phase transition curve might be the explanation. In contrast, *Gautron et al.* [1996] synthesized these solid phases with large sizes, and observed partial melting at much lower *T* (from 1400 to 1600°C). Potentially, their experimental charges contained small amounts of water, which was also suggested by the high Al_2O_3 content in the St [*Gautron et al.*, 1996; *Liu et al.*, 2006].

[14] We observed one subsolidus phase assemblage (CAS + CaPv + St) and one supersolidus phase assemblage (CAS + CaPv + Melt) in the experiments at 22 GPa (from 1600 to 2400°C). Therefore, St is the first phase to melt out. The submicron grain sizes in OS-1378 (Table 1) are extremely unusual, which has not been well explained so far.

[15] The experiments at 25 GPa (from 1600 to 2000°C; Table 1) produced the subsolidus phase assemblage CAS + CaPv + St as well, but behaved much better than those at 22 GPa: the higher the experimental *T*, the larger the grain size. As will be disclosed later, the CAS phase in OS-1269 shows large compositional variation.

[16] The phase relations of the An composition at high *P-T* conditions are summarized in Figure 3. The consecutive subsolidus phase assemblages, from ambient *P* to the *P* condition of the uppermost lower mantle of the Earth (up to ~25 GPa), are An, Gr + Ky + Qz, Gr + Ky + Coe, Gr + Ky + St, Gr + CAS + St and CAS + CaPv + St. As will be clear later, the phase assemblage CAS + CaPv + St will be replaced by the phase assemblage St + Cor + CaPv at about 26 GPa (subject to *T*). The partial melting process of

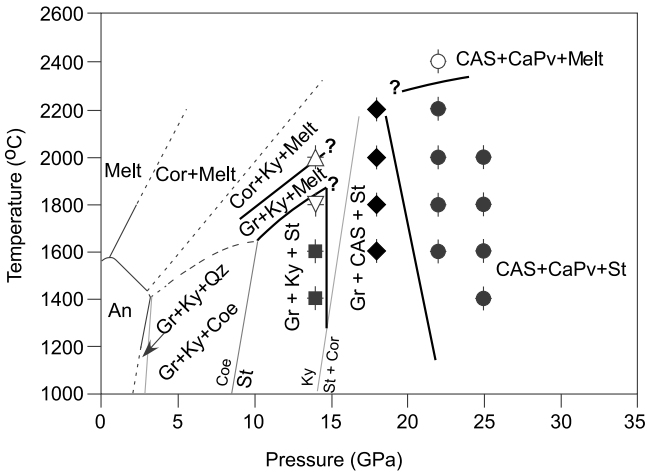

Figure 3. Phase relations of the An composition at high *P-T* conditions. An, anorthite; Gr, grossular; Ky, kyanite; Qz, quartz; Coe, coesite; St, stishovite; Cor, corundum; CAS, calcium-alumino-silicate phase; CaPv, Al_2O_3-bearing calcium perovskite. Filled symbols are for subsolidus experiments whereas empty symbols are for supersolidus experiments. Thick solid curves are determined in this study, thin solid curve for the reaction Ky→St + Cor is from *Liu et al.* [2006], and other thin solid or broken curves are from *Presnall* [1995].

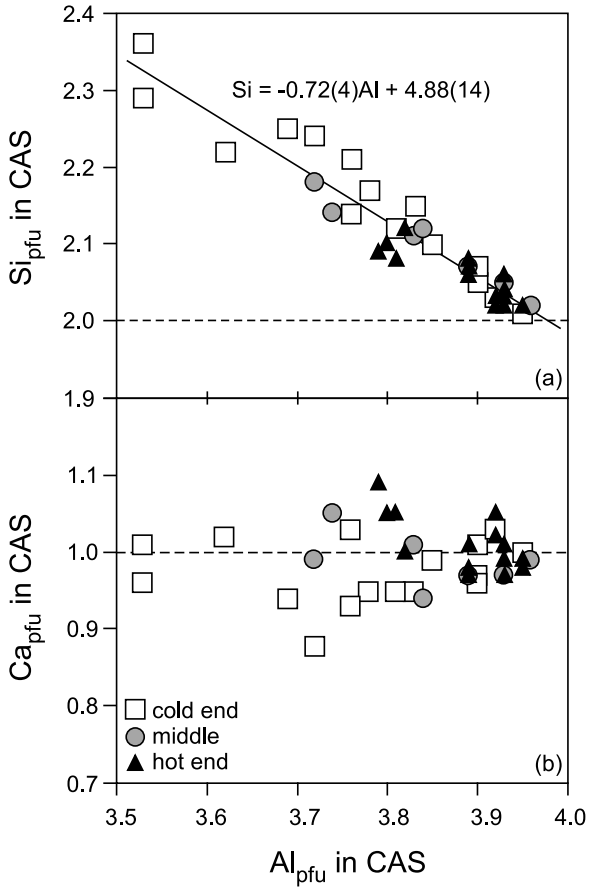

Figure 4. Composition of the CAS phase in OS-1269 (in molar units). pfu, per formula unit. The horizontal broken lines indicate the contents of Si and Al in the commonly assumed chemical formula $CaAl_4Si_2O_{11}$ of the CAS phase [*Gautron et al.*, 1996].

the An composition is largely unconstrained, with the only concrete result that St is the first phase to melt out for the experimentally covered *P* range. At 14 GPa, the supersolidus phase assemblages are tentatively established as Gr + Ky + St + Melt, Gr + Ky + Melt, Cor + Ky + Melt, Cor + Melt, and finally Melt.

[17] In general, the Al_2O_3 content in St is about 1 wt%, somewhat lower than that of St in *Liu et al.* [2006]. Unlike in *Liu et al.* [2006], it does not clearly correlate with *P* or *T*, presumably suggesting a strong influence of the coexisting phases (Table 1). To the contrary, St in *Liu et al.* [2006] always coexisted with Cor, so that its Al_2O_3 content should have been buffered and maximized by Cor.

[18] Cor was observed in OS-1278 only. Its SiO_2 content is about 2 wt%, in good agreement with *Liu et al.* [2006]. One interesting phenomenon about Cor is that it contains about 1 wt% MgO (Table 2), compatible to the observation made by *Litasov and Ohtani* [2010].

[19] Ky in general is compositionally close to its ideal chemical formula, Al_2SiO_5. The small amount of CaO might indicate contamination in the chemical analyses caused by the usually small grain size of Ky (up to ~0.2 wt%; OS-1253 in Table 2). Indeed, Ky with large grain size from OS-1278 is essentially CaO-free. On the other hand, Ky from OS-1278 contains ~0.3 wt% MgO, much compatible to the observations of *Rapp et al.* [2008] and *Litasov and Ohtani* [2010].

[20] Gr was observed in the experiments at 14 and 18 GPa (Table 1). Compared to the ideal chemical formula of Gr ($Ca_3Al_2Si_3O_{12}$), our Gr is generally richer in Si and Al, but poorer in Ca (Table 2), in good agreement with *Gautron et al.* [1996]. In addition, the total of the ions calculated on the basis of 12 oxygens is less than 8, indicating the possible presence of vacancy in the Gr crystal structure. However, we were not able to establish the substitution mechanism due to the poor quality of the Gr composition data collected on the small grains in some experiments (Table 1).

[21] CAS phase was first observed by *Irifune et al.* [1994]. Its general chemical composition was later established as $CaAl_4Si_2O_{11}$ by *Gautron et al.* [1996] whereas its detailed structural characteristics were intensively investigated by *Gautron et al.* [1997, 1999], *Grey et al.* [1999], and *Xue et al.* [2009]. Recently, *Ono et al.* [2005], *Liu et al.* [2011], and *Gréaux et al.* [2011a] studied its equation of state up to ~44 GPa. Its high *P-T* phase relationships were examined in *Ishibashi et al.* [2008], *Zhai and Ito* [2008], and *Akaogi et al.* [2009]. However, its potential composition variation at high *P-T* conditions has not been critically evaluated to date, despite *Hirose and Fei* [2002] demonstrated that its composition might significantly deviate from $CaAl_4Si_2O_{11}$. We arbitrarily selected OS-1269 and extensively collected composition data for the CAS grains at different portions of the sample (Table 2). Figure 4 shows the following points: (1) Al in the CAS phase is extensively replaced by Si alone whereas the Ca content is rather constant, so that the Si/Ca molar ratio will become larger than 2; (2) the replacing mechanism, approximately $3Si^{4+} = 4Al^{3+}$, will lead to vacancies in the CAS structure, which is verified by our composition data acquired from other samples (Table 2); (3) the composition of the CAS, coexisting with other silicate phases, is strongly affected by *T*, but probably only slightly affected by *P* (Table 2).

[22] The melts observed in our experiments are generally andesitic, in good agreement with those observed by *Gautron et al.* [1996]. At both 14 and 22 GPa, St is the first phase to melt out, so that the SiO_2 content of the melts along the solidus is high. However, due to the severe quench modification caused by the low melt fraction (OS-1247) or Soret effect resulted in by the large *T* gradient (OS-1278), large compositional variation was present in our analyses.

4. Subsolidus Reactions and Partial Melting Behavior

[23] For the investigated *P* interval, there are three subsolidus phase assemblages, Gr + Ky + St, Gr + CAS + St and CAS + CaPv + St, so that two subsolidus reactions are involved in this phase transition process.

[24] As indicated in Figure 5a, the first subsolidus reaction is

$$Ca_3Al_2Si_3O_{12}(Gr) + 5Al_2SiO_5(Ky) = 2SiO_2(St) + 3CaAl_4Si_2O_{11}(CAS), \quad (1)$$

assuming that all involved phases are compositionally close to their chemical formulas. For the An composition, the phase proportion in the phase assemblage Gr + Ky + St is Gr:Ky:

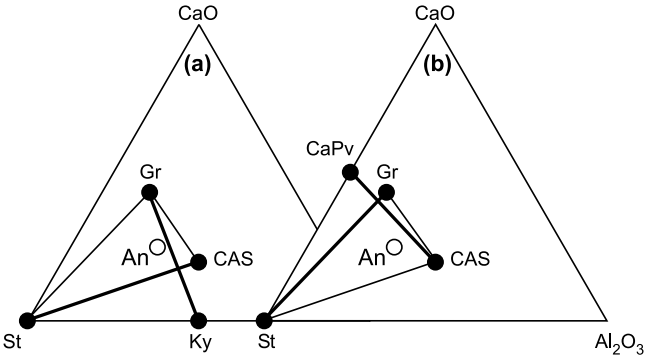

Figure 5. Subsolidus phase reactions for the An composition: (a) Gr + Ky → St + CAS at ~14 GPa relating the low-*P* phase assemblage Gr + Ky + St and high-*P* phase assemblage Gr + CAS + St and (b) Gr + St → CAS + CaPv at ~20 GPa relating the low-*P* phase assemblage Gr + CAS + St and high-*P* phase assemblage CAS + CaPv + St. All possible solid solution behaviors are ignored. Phase compositions are shown in molar units.

St = 1:2:1 (by mole), so that equation (1) should lead to the elimination of Ky, and the formation of the phase assemblage Gr + CAS + St. It is well known that Ky breaks down to the phase assemblage St + Cor at about 15 GPa [*Liu*, 1974; *Irifune et al.*, 1995; *Schmidt et al.*, 1997; *Liu et al.*, 2006; *Ono et al.*, 2007], which actually does not play any role in the phase transition of the An composition for the *T* interval covered by our experiments.

[25] According to Figure 5b, the second subsolidus reaction is

$$2Ca_3Al_2Si_3O_{12}(Gr) + SiO_2(St) = CaAl_4Si_2O_{11}(CAS) + 5CaSiO_3(CaPv) \quad (2)$$

assuming that all involved phases are compositionally close to their chemical formulas. For the An composition, the phase proportion in the phase assemblage Gr + CAS + St is Gr:CAS:St = 1:2:3 (by mole), so that equation (2) should lead to the elimination of Gr, and the formation of the phase assemblage CAS + CaPv + St (CAS:CaPv:St = 1:1:1; by mole).

[26] As observed in OS-1247 at 14 GPa, the phase assemblage Gr + Ky + St starts to melt at about 1800°C. From the consideration of mass balance, Figure 6a suggests a melting reaction in the following form:

$$St + Gr \rightarrow Ky + Melt, \quad (3)$$

with St as the first solid phase to be eliminated. By using the real phase compositions listed in Table 2 (plus, assuming 1 wt% Al_2O_3 in St) and following the method outlined in *Korzhinskii* [1959] and *Walter et al.* [1995], we obtain the partial melting reaction as shown below:

$$0.23St + 0.87Gr = 0.11Ky + 1Melt, \quad (4)$$

with all coefficients of the phases normalized to the coefficient of Melt (wt%). Before this melting reaction, the phase proportion for the An composition is Gr:Ky:St = 0.56:0.38:0.07 (wt%); after this melting reaction, it is Gr:Ky:Melt = 0.32:0.40:0.28 (wt%).

[27] Further partial melting at 14 GPa (OS-1278), however, has not been definitely constrained due to the large compositional variation of the melts caused by the potential Soret effect (Figure 2b). If the melt composition from the low-*T* part of the clear melt area (55.3% SiO_2, 17.06% Al_2O_3, 3.15% MgO and 24.49% CaO by weight; Composition A in Figure 6b, with MgO ignored) is used to calculate the melting reaction, following the same method as mentioned above, we arrive at the following reaction:

$$0.72Gr + 0.76Ky = 0.48Cor + 1Melt, \quad (5)$$

with all coefficients normalized to the coefficient of Melt (wt%). For the An composition, the phase proportion before this reaction takes place is Gr:Ky:Melt = 0.32:0.40:0.28 (wt%), so that equation (5) would lead to the elimination of Gr, resulting in a phase proportion of Cor:Ky:Melt = 0.28:

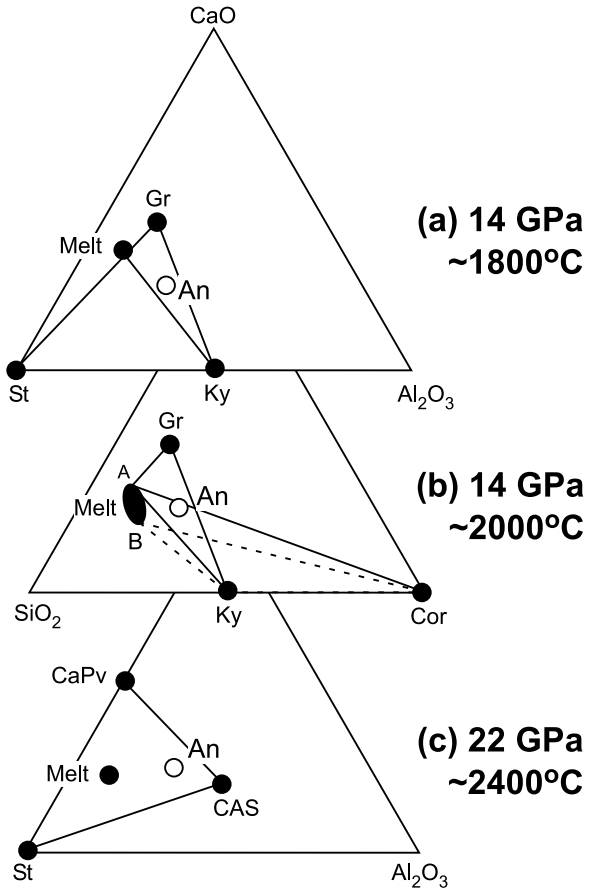

Figure 6. Melting reactions for the An composition: (a) St + Gr→Ky + Melt (14 GPa), (b) Gr + Ky→Cor + Melt (Composition A; 14 GPa), and (c) CAS + CaPv + St→Melt (22 GPa). All possible solid solution behaviors are ignored. Phase compositions are shown in molar units. Note the spread of the melt composition in Figure 6b, with Composition A from the low-*T* part of the clear melt while Composition B from the high-*T* part. As indicated by the broken triangle, the An composition cannot be mass balanced by the phase assemblage Cor + Ky + Melt (Composition B), suggesting potential Soret effect which increased the Al_2O_3 content but decreased the CaO content of the high-*T* end of the experimental charge.

(−0.08):0.80 (wt%). Although the melting reaction agrees with our direct phase observation (coexisting Cor, Ky and Melt), the negative phase proportion of Ky after the elimination of Gr indicates the discrepancy in the compositional data, which is mostly caused by the uncertainty in the melt compositional data influenced by the Soret effect. If the CaO content of the melt composition used in the above calculation is increased by 2% and Al_2O_3 content correspondingly reduced by 2% (Figure 2b), tentatively, the calculated phase proportion is Cor:Ky:Melt = 0.25:0.01:0.74 (wt%), a solution suggesting Gr as the second phase to melt out. In addition, we can use the melt composition from the high-T part of the clear melt area (55.72% SiO_2, 22.90% Al_2O_3, 2.55% MgO and 18.83% CaO by weight; Composition B in Figure 6b, with MgO ignored) to tentatively calculate the phase proportion of Cor:Ky:Melt at relatively high T for the An composition, which leads to a large negative number for Ky. Two conclusions can be drawn from this exercise: (1) following St and Gr, Ky is likely the third phase to melt out, and the resulting phase assemblage is Cor + Melt; (2) since Ky, Cor and Melt have lower CaO content than An (20.16 wt%), some migration of CaO from the high-T part to low-T part of the clear melt area must have occurred in this experiment, indicating the role of the Soret effect.

[28] We do not have any data to illustrate the partial melting behavior of the phase assemblage Gr + CAS + St. According to *Gautron et al.* [1996], the melting reaction is peritectic, and in the form as follows:

$$\mathrm{Gr} + \mathrm{St} \rightarrow \mathrm{CAS} + \mathrm{Melt}, \quad (6)$$

which leads to the elimination of St, for the composition of An.

[29] As to the partial melting process of the phase assemblage CAS + CaPv + St (22 GPa), the composition data suggest the following reaction:

$$0.22\mathrm{CAS} + 0.37\mathrm{CaPv} + 0.40\mathrm{St} = 1\mathrm{Melt}, \quad (7)$$

with all coefficients normalized to the coefficient of Melt (wt%). Distinctly, the melting reaction for this phase assemblage is eutectic type, rather than peritectic type (Figure 6c). Before this melting reaction, the phase proportion for the An composition is CAS:CaPv:St = 0.65:0.24:0.11 (wt%), so that St should be the first solid phase to melt out, according to equation (7).

5. Chemistry of CAS

[30] The composition of the CAS phase was first established as $CaAl_4Si_2O_{11}$ [*Gautron et al.*, 1996]. However, *Irifune et al.* [1994], *Hirose and Fei* [2002], and *Hirose et al.* [2004] demonstrated the incorporation of other components into the CAS structure and its significant compositional deviation from the $CaAl_4Si_2O_{11}$ formula. With the experimental investigation in the system $CaAl_4Si_2O_{11}$-$NaAl_3Si_3O_{11}$ by *Akaogi et al.* [2010], it is clear now that the CAS phase is actually a complex solid solution. The highest contents of Fe_{pfu}, Mg_{pfu}, Na_{pfu} and K_{pfu} observed in high-P experiments are 0.308 [*Grassi and Schmidt*, 2011], 0.388 [*Keshav and Gudfinnsson*, 2010], 0.524 [*Akaogi et al.*, 2010] and 0.323 [*Grassi and Schmidt*, 2011], respectively. On the other hand, the contents of Ti_{pfu} (up to 0.068), Cr_{pfu} (up to 0.005) and Mn_{pfu} (up to 0.002) are generally negligible [*Hirose and Fei*, 2002; *Hirose et al.*, 2004; *Grassi and Schmidt*, 2011]. The CAS phase observed in the Martian meteorites by *Beck et al.* [2004] has distinctly high Na_{pfu}, ∼0.83.

[31] A few substitution mechanisms have been proposed to explain the CAS solid solution. *Hirose and Fei* [2002] suggested the tripled substitution between SiSiNa and AlAlAl while *Akaogi et al.* [2010] clearly demonstrated the coupled substitution between SiNa and AlCa. Our study here indicates another substitution mechanism, 3Si → 4Al (Figure 4).

[32] To better understand the CAS solid solution, we collect all the available composition data, and show them in Figure 7 (41 data points; molar unit). The composition data from the system CaO-Al_2O_3-SiO_2 (CAS system; 16 data points) demonstrate the substitution between 3Si and 4Al, and those from the system CaO-Al_2O_3-SiO_2-Na_2O (CAS-Na system; 7 data points) suggest the substitution of Si + Na→Al + Ca. There were only two composition data in the system CaO-MgO-Al_2O_3-SiO_2 (CMAS system) [*Keshav and Gudfinnsson*, 2010], and two composition data in the system CaO-MgO-Al_2O_3-SiO_2-Na_2O (CMAS-Na system) [*Litasov and Ohtani*, 2010]. Note that the investigated systems in *Keshav and Gudfinnsson* [2010] and *Litasov and Ohtani* [2010] actually contained CO_2 which might have some minor effects on the compositions of the CAS phase; but since these four data were the only available data in these systems, we chose to ignore the CO_2 effect. Thanks to the work of *Akaogi et al.* [2010], we were able to remove the Na_2O effect from those two data in the CMAS-Na system. Then we arrived at four data points for the nominal CMAS system, which suggest the substitution mechanism of 2Si + Mg + Ca→4Al (in other words, Si + Mg → 2Al and Si + Ca→2Al). It appears, therefore, that the presence of Mg brings Ca into the cation-substituting process. If we add all the substitution mechanisms together, we obtain 6Si + Na + Mg + Ca→9Al + Ca (or 6Si + Na + Mg→9Al), which can be used to explain the compositional variation of the CAS phases observed in the natural rock compositions at high P.

[33] There are in total 14 composition data reported for the CAS phase by the high-P experiments with natural rock compositions [*Irifune et al.*, 1994; *Hirose and Fei*, 2002; *Hirose et al.*, 2004; *Grassi and Schmidt*, 2011]. Due to their low concentrations, Ti has been added to Si, Cr to Al, Fe and Mn to Mg, and K to Na, which reduces the number of the composition variables to 5. The reduced data are shown in Figure 7. Apart from one data point (Fe_{pfu} = 0.308) [*Grassi and Schmidt*, 2011], all other data points fall close to a straight line, suggesting that some substitution mechanism really operates. The slope of the correlation line, −0.40, approximates that defined by the data in the nominal CMAS system (−0.49), indicating the dominant role of the substitution mechanism of 2Si + Mg + Ca = 4Al (or, Si + Mg → 2Al and Si + Ca→2Al) for the specific composition range covered by these data points. To better constrain the role of Fe, the CAS phase enriched in Fe deserves further experimental investigation. Figure 7 also shows the composition of the CAS phase observed in the Martian meteorites [*Beck et al.*, 2004]. Because it is enriched in Na, it plots away from the trend defined by the experimental data, suggesting

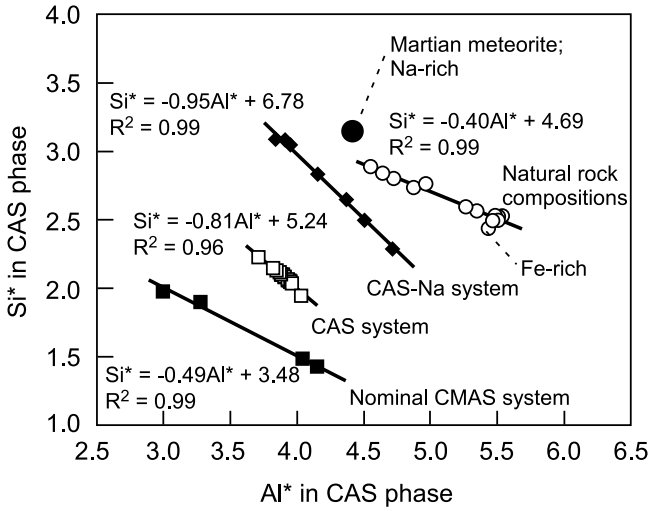

Figure 7. Compositional correlations between Si* and Al* of the CAS phases from different composition systems (in molar units and on the basis of 7 oxygens). In the CAS system [*Gautron et al.*, 1996; *Zhai and Ito*, 2008; *Gréaux et al.*, 2011b; this study], Si* = Si_{pfu} and Al* = Al_{pfu}. In the CAS-Na system [*Akaogi et al.*, 2010], Si* = Si_{pfu} + Na_{pfu} and Al* = Al_{pfu} + Ca_{pfu}. In the nominal CMAS system [*Litasov and Ohtani*, 2010; *Keshav and Gudfinnsson*, 2010], Si* = $0.5Si_{pfu}$ + $0.5(Ca_{pfu} + Mg_{pfu})$ and Al* = Al_{pfu}. In the natural rock composition systems [*Irifune et al.*, 1994; *Hirose and Fei*, 2002; *Hirose et al.*, 2004; *Grassi and Schmidt*, 2011] and for the Martian meteorites [*Beck et al.*, 2004], Si* = $(6Si_{pfu} + 6Ti_{pfu} + Na_{pfu} + Ca_{pfu} + Mn_{pfu} + Mg_{pfu} + Fe_{pfu})/6$ and Al* = $(9Al_{pfu} + 9Cr_{pfu} + Ca_{pfu})/6$.

the importance of a different substitution mechanism, most likely Si + Na→Al + Ca [*Akaogi et al.*, 2010].

6. Chemistry of CaPv

[34] In most cases CaPv is not quenchable [*Liu and Ringwood*, 1975; *Mao et al.*, 1977; *Irifune*, 1994], so that its chemical characteristics are still unclear. Figure 8 summarizes the compositional data of CaPv from the CaO-MgO-SiO_2 system (CMS system), CAS system, CaO-MgO-Al_2O_3-SiO_2-FeO system (CMAS-Fe system), and more complicated composition systems such as the basaltic compositions and peridotitic compositions. The compositional data of some CaPv which did not coexist with any other silicate phases are deliberately left out [*Fitz Gerald and Ringwood*, 1991; *Bläß et al.*, 2004; *Kojitani et al.*, 2009]. CaPv without full compositional characterization is also excluded [*Irifune et al.*, 2000; *Takafuji et al.*, 2002].

[35] Figure 8a suggests that some of the CaPv from the CAS system have very high Al_2O_3 content [*Gautron and Madon*, 1994; *Gréaux et al.*, 2011b], which is questionable. The good linear relations between Al and Si (Figure 8a; 5 data points in total) and between Ca and Si (Figure 8b; 5 data points in total) lead to the following substitution mechanism:

$$2Al^{3+} = Si^{4} + Ca^{2+}, \quad (8)$$

so that the CaPv formula can be represented by $Ca_{1-0.5x}Al_xSi_{1-0.5x}O_3$. To maintain the charge balance, no oxygen vacancy is required, which possibly explains why *Gréaux et al.* [2011b] could not fit their CaPv to the oxygen-deficient

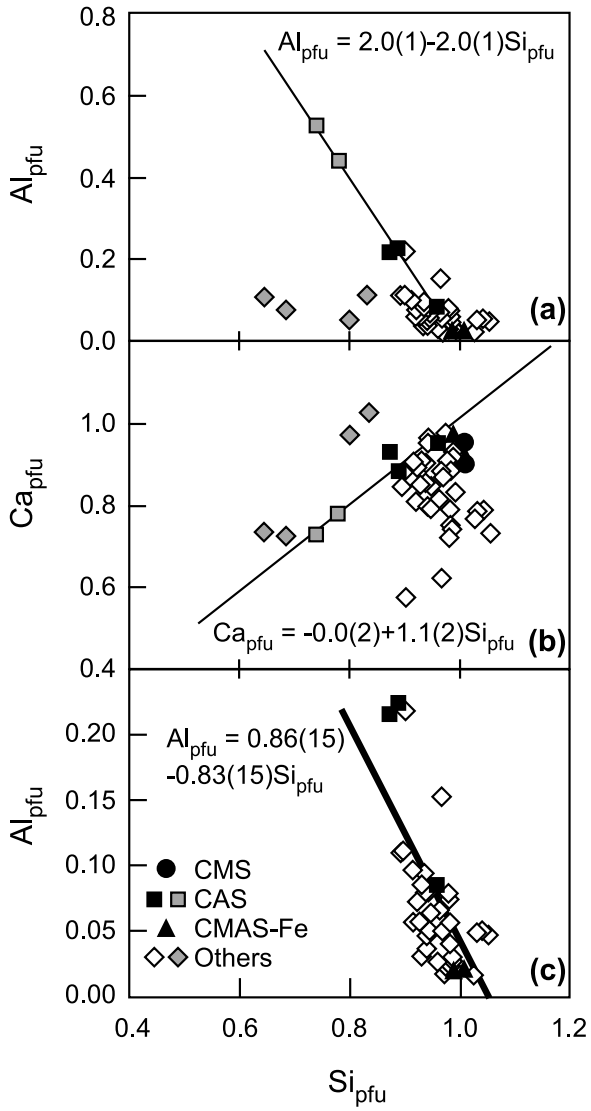

Figure 8. Compositions of CaPv: (a) Al_{pfu} versus Si_{pfu} for all data, (b) Ca_{pfu} versus Si_{pfu} for all data, and (c) Al_{pfu} versus Si_{pfu} for the data set with 6 data points removed. Data source: *Akaogi et al.* [2004b] (CMS system), *Gréaux et al.* [2011b] (CAS system), *Gautron and Madon* [1994] (CAS system), *Litasov and Ohtani* [2003] (CMAS system), *Asahara et al.* [2005] (CMAS-Fe system), *Kesson et al.* [1994] (basalt), *Funamori et al.* [2000] (basalt), *Hirose and Fei* [2002] (basalt), *Hirose et al.* [2004] (MORB and peridotite), *Irifune and Ringwood* [1993] (MORB), *Ono et al.* [2001] (MORB), *Okamoto and Maruyama* [2004] (MORB + H_2O), *Hirose et al.* [2005] (MORB), *Ricolleau et al.* [2008] (MORB), *Irifune* [1994] (pyrolite), *Kesson et al.* [1998] (pyrolite), and *Wood* [2000] (peridotite). Data represented by the gray symbols in Figures 8a and 8b are removed in Figure 8c. Correlation line in Figures 8a and 8b is regressed from the five data points (the gray and dark squares) in the CAS system only whereas that in Figure 8c is from all shown data points.

models of CaPv [*Bläß et al.*, 2004; *Kojitani et al.*, 2009]. With $x = 0.5$, the composition of the CaPv should be $Ca_{0.75}Al_{0.5}Si_{0.75}O_3$, which is isochemical to $Ca_3Al_2Si_3O_{12}$, the composition of Gr. With $x = 2$, the composition of the CaPv should be Al_2O_3, the composition of Cor. Since the MA experiments in the CAS system [*Gréaux et al.*, 2011b] were either done with a glass starting material of the Gr composition at very low T (OS1777 at 1127°C for 4 h), or done with the Gr starting material (S2152 at 1427°C for a few minutes; OS1714 at 1727°C for 10 h), and since the diamond-anvil cell (DAC) experiment was done with an anorthite starting material which is rich in Al_2O_3 [*Gautron and Madon*, 1994], we tend not to believe that all these experiments reached their full chemical equilibrium, and that the removal of Al_2O_3 from the Gr or An composition was fully achieved in all cases. Indeed, the MA experiments carried out by *Takafuji et al.* [2002] with a Gr starting material demonstrated that the Al_{pfu} of their stable CaPv was only ~0.12–0.16 whereas that of their metastable CaPv reached ~0.4–0.5. Therefore, it appears that the substitution mechanism, equation (8), is probably an artifact, which deserves more experimental work. In order to disclose the real substitution mechanism of Al in CaPv, we have to remove from the data set at least those two data points with the highest Al_2O_3 contents (Figure 8a; $Al_{pfu} = 0.44$ [*Gautron and Madon*, 1994] or 0.53 [*Gréaux et al.*, 2011b]), and we can subsequently conclude that the Al_{pfu} of the CaPv in equilibrium with other silicate phases seldom exceeds 0.2.

[36] Figure 8b shows not only the good relation between the Ca and Si of the CaPv in the CAS system, but also the important fact that the CaPv in equilibrium with other silicate phases usually contains less Ca than Si. This should be expected since CaPv is usually the most Ca-rich phase, and since the bulk compositions of the geologically significant systems such as the basaltic and peridotitic compositions have much lower CaO contents. Among the 5 data points which nominally show higher Ca than Si, 3 data points were due to the high TiO_2 content (up to about 24 wt%) which replaces Si [*Ono et al.*, 2001; *Okamoto and Maruyama*, 2004], one data point was probably due to a typing mistake (the SiO_2 and total are about 10% lower than other analyses) [*Hirose and Fei*, 2002], and one data point was mainly due to the slight chemical disequilibrium as discussed above [*Gréaux et al.*, 2011b]. In addition, Figure 8b does not show any clear correlation between the Ca and Si contents of the CaPv from the high-P experiments done with the natural rock compositions, suggesting that the charge-coupled substitution mechanism (equation (8)) does not play a leading role.

[37] With the further removal of the 4 data points of the complex compositions, 3 with very high TiO_2 content and 1 with possible typing mistake, we came up with a data set which contains 41 composition data for CaPv, covering P from ~21 to 135 GPa and T from ~1000 to 2500°C. Different tests were conducted to seek the correlations between Al and other components, leading to Figure 8c which likely demonstrates a pattern. This pattern is controlled by the CaPv data from the natural composition systems, rather than the CaPv data from the simple systems. If Si is added with Ti which in general replaces Si, the compositional data of the CaPv from the simple and natural rock composition systems become well mixed, defining a slightly better relationship as follows:

$$Al_{pfu} = 1.06(15) - 1.02(15) \times \left(Si_{pfu} + Ti_{pfu}\right). \quad (9)$$

In spite of the potential effects from other components, equation (9) suggests that Al in CaPv in equilibrium with other silicate phases mainly replaces Si by equal moles. This substitution mechanism then should lead to the formation of oxygen vacancy (O_v^{2+}) in the CaPv structure, in order to balance the charges ($Si^{4+} \rightarrow Al^{3+} + 0.5\ O_v^{2+}$).

[38] Tests were also conducted to constrain the effect of P or T on the substitution mechanism, but led to no clear-cut conclusion. The Ca + Mg + Fe + Mn content of the CaPv seems constant with respect to the P variation, suggesting a minor influence of pressure on the charge-coupled substitution mechanism (equation (8)), if this mechanism operates in the first place. On the other hand, the magnitude of the (Al + Cr)/(Si + Ti) ratio of the CaPv is gradually reduced by P, presumably implying that the oxygen vacancy-forming mechanism ($Si^{4+} \rightarrow Al^{3+} + 0.5\ O_v^{2+}$) is suppressed to some extent by high P.

[39] Summarily, the incorporation of Al into the CaPv coexisting with other silicate phases is mostly controlled by the oxygen vacancy-forming mechanism ($Si^{4+} \rightarrow Al^{3+} + 0.5\ O_v^{2+}$), rather than by the charge-coupled substitution mechanism (equation (8)). For the CaPv from the simple systems such as the CAS system, the charge-coupled substitution ($2Al^{3+} = Si^{4+} + Ca^{2+}$) may not be very important as well, which is very different to the case of magnesium perivoskite (MgPv) in the system $MgO\text{-}Al_2O_3\text{-}SiO_2$ (MAS). The incorporation of Al into the MgPv in the MAS system is dominated by the charge-coupled substitution mechanism ($2Al^{3+} = Si^{4+} + Mg^{2+}$), as suggested by the high-P experiments of *Walter et al.* [2004, 2006].

7. Some Subsolidus Phase Relations in the CAS System

[40] With the experimental results from this investigation, and those from *Irifune et al.* [1995], *Schmidt et al.* [1997], *Liu et al.* [2006], *Ono et al.* [2007], *Zhai and Ito* [2008], *Ishibashi et al.* [2008], and *Akaogi et al.* [2009], we followed the method of Schreinemakers [*Schreinemakers*, 1915; *Zen*, 1966] to construct the P-T phase diagram for a portion of the CAS system (Figure 9a). For the P interval from 10 to ~25 GPa, three subsolidus divariant phase assemblages (Gr + Ky + St, Gr + CAS + St and CAS + CaPv + St) have been observed for the An composition, so that we can generally assume that there are at least two invariant points to relate these phases. Specifically, Gr, Ky, St, Cor and CAS form the unique phase assemblage for the invariant point I_1 whereas Gr, St, Cor, CAS and CaPv form the unique phase assemblage for the invariant point I_2.

[41] For the 5 univariant curves originating from the invariant point I_1, a degeneracy occurs due to the compositional collinearity among St, Cor and Ky (Figure 9b), so that the five univariant curves have only 4 distinct slopes. The five univariant reactions are:

$$(Ky)CAS = Cor + Gr + St, \quad (10)$$

$$(Cor)Gr + Ky = St + CAS, \quad (11)$$

$$(St)CAS = Cor + Gr + Ky, \quad (12)$$

$$(Gr)Ky = Cor + St, \quad (13)$$

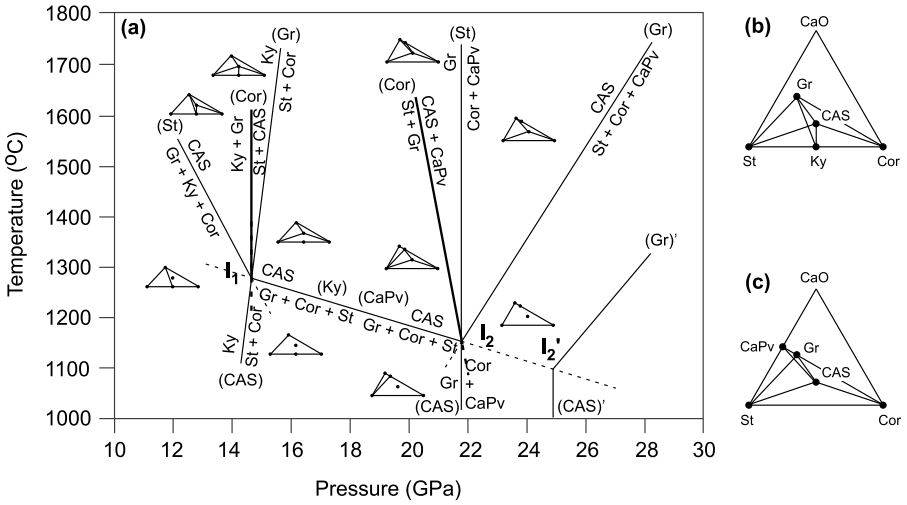

Figure 9. *P-T* phase diagram of a portion of the CAS system: (a) the *P-T* phase diagram, (b) the compositional relations of the phases present at invariant point I_1, and (c) the compositional relations of the phases present at invariant point I_2. The thermodynamically calculated phase reactions of CAS = St + Cor + CaPv and Gr = Cor + CaPv [*Akaogi et al.*, 2009] are labeled as (Gr)′ and (CAS)′, respectively; their interception point is labeled as I'_2, which is expected to coincide with I_2. Two univariant phase boundaries of [Cor] at ~14 GPa and [Cor] at ~19 GPa, as shown by the thick curves, are constrained by this experimental investigation.

and

$$(\mathrm{CAS})\mathrm{Ky} = \mathrm{Cor} + \mathrm{St}, \tag{14}$$

with the reaction (Gr) identical to the reaction (CAS). For all these reactions, (Gr) or (CAS) has been investigated by *Irifune et al.* [1995], *Schmidt et al.* [1997], *Liu et al.* [2006], and *Ono et al.* [2007], (Ky) and (St) have been investigated by *Zhai and Ito* [2008] and *Akaogi et al.* [2009], and (Cor) has been investigated by this study (equation (1)). Therefore, the phase relations around the invariant point I_1 have been fully determined.

[42] For the 5 univariant curves originating from the invariant point I_2, a degeneracy also occurs due to the compositional collinearity among CaPv, Cor and Gr (Figure 9c), so that the five univariant curves have only 4 distinct slopes. The five univariant reactions are:

$$(\mathrm{CaPv})\mathrm{CAS} = \mathrm{Cor} + \mathrm{Gr} + \mathrm{St}, \tag{15}$$

$$(\mathrm{Cor})\mathrm{Gr} + \mathrm{St} = \mathrm{CAS} + \mathrm{CaPv}, \tag{16}$$

$$(\mathrm{Gr})\mathrm{CAS} = \mathrm{Cor} + \mathrm{St} + \mathrm{CaPv}, \tag{17}$$

$$(\mathrm{St})\mathrm{Gr} = \mathrm{Cor} + \mathrm{CaPv}, \tag{18}$$

and

$$(\mathrm{CAS})\mathrm{Gr} = \mathrm{Cor} + \mathrm{CaPv}, \tag{19}$$

with the reaction (St) identical to the reaction (CAS). For all these reactions, (CaPv), which is identical to the reaction (Ky) originating from the invariant point I_1, was investigated by *Zhai and Ito* [2008] and *Akaogi et al.* [2009], and (Gr) investigated by *Ishibashi et al.* [2008], and (Cor) investigated by this study (equation (2)). Therefore, the phase relations around the invariant point I_2 have been almost completely determined, with the slope of the reaction (St) or (CAS) as the only exception. There is a 4 GPa difference for the *P-T* loci of the reaction (Gr), as experimentally determined by *Ishibashi et al.* [2008] and thermodynamically calculated by *Akaogi et al.* [2009]. Overall, the experimental determination appears more compatible to other data, suggesting that some of the thermodynamic data used in *Akaogi et al.* [2009] should be further refined.

[43] Since St, Cor, and CaPv do not break down to any other simpler chemical forms up to at least the pressure at the core-mantle boundary of the Earth, the phase assemblage St + Cor + CaPv is applicable to the An composition, and to a portion of the CAS system under the lower mantle *P-T* conditions, if further isochemical phase transitions of the individual phase are ignored [*Kingma et al.*, 1995; *Dubrovinsky et al.*, 1997; *Funamori and Jeanloz*, 1997; *Andrault et al.*, 1998].

[44] It concludes that for the An composition the subsolidus phase assemblages (at 1200°C for example) should be An (~0–2.5 GPa), Gr + Ky + Qz (~2.5–3.0 GPa), Gr + Ky + Coe (~3.0–9 GPa), Gr + Ky + St (~9–14.5 GPa), Gr + Cor + St (~14.5–20 GPa), Gr + CAS + St (~20–21.5 GPa), CAS + CaPv + St (~21.5–22 GPa), and St + Cor + CaPv (>22 GPa), as *P* increases from ambient *P* to the *P* at the core-mantle boundary of the Earth (Figures 3 and 9). This result is in excellent agreement with early related investigations at similar temperatures [*Boyd and England*, 1961; *Hays*, 1966; *Hariya and Kennedy*, 1968; *Reid and Ringwood*, 1969; *Gautron et al.*, 1996]. At very high *T*, *Madon et al.* [1989] and *Gautron and Madon* [1994] used An as the starting material to carry out some laser-heated DAC experiments. They found a phase assemblage of $Ca_{1.33}Al_{1.33}Si_{2.33}O_8$ (hollandite-type structure) + Al_2SiO_5 (distorted Ky structure) + $Ca_{0.8}Al_{0.4}Si_{0.8}O_3$ (amorphous

CaPv) at $P > \sim$10 GPa and $T > \sim$1500°C, which is not in agreement with our observation made here and other related experimental studies in the literature [*Irifune et al.*, 1995; *Gautron et al.*, 1996; *Schmidt et al.*, 1997; *Liu et al.*, 2006; *Ono et al.*, 2007].

8. High-*P* Behavior of Gr Composition

[45] Garnet is one of the most important constituent minerals for basaltic and peridotitic compositions at high *P*. Gr is a very important end-member of garnet solid solutions, so that its high *P-T* behavior has been extensively explored [*Mao et al.*, 1977; *Liu*, 1979; *Ahmed-Zaïd and Madon*, 1995; *Yusa et al.*, 1995; *Takafuji et al.*, 2002; *Gréaux et al.*, 2011b]. Due to the well-known slow cation diffusion in the garnet crystal structure, as exemplified by the ubiquitous compositional zoning in natural garnets, large discrepancies exist in the experimental literature. In the 1970s, taking as one example, *Mao et al.* [1977] reported the phase assemblage of Cor + CaPv (unquenchable) whereas *Liu* [1979] reported a tetragonal phase with the Gr composition for similar *P-T* conditions (~30 GPa and 1000°C). In the last decade or so, taking as another example, *Takafuji et al.* [2002] experimentally demonstrated that Gr decomposes to the phase assemblage CaPv + Cor whereas *Gréaux et al.* [2011b] argued for the stable phase assemblage Gr + CaPv at similar *P-T* conditions (22–25 GPa and ~800–1000°C). These discrepancies might have been caused by the sluggish nature of cation diffusion in the Gr structure, short heating durations in the high-*P* experiments (especially in the laser-heated DAC experiments), and deviation of starting composition from the ideal Gr composition.

[46] Our high-*P* experiments with the An composition were performed under very high temperatures, and with long experimental durations, so that the experimental charges should have closely approached their chemical equilibrium, and that the experimental results should be highly reliable. As analyzed above, these experimental results, combined with the literature data about some relevant compositions, have led to a well determined *P-T* phase diagram for a portion of the CAS system. Since the difference between the An composition and Gr composition is small, this phase diagram is also applicable to the case of the Gr composition under high *P*.

[47] Figure 9 clearly suggests that at 1000°C, Gr is stable up to ~21.5 GPa, and then decomposes to the phase assemblage Cor + CaPv [univariant reaction curve (CAS) originating from the second invariant point I_2]. Whatever the slope of the univariant reaction curve (CAS) is, the constraints from the univariant reaction curves (Cor) and (Gr) dictate that the maximum variation of the transition *P* of the univariant reaction curve (CAS) at 1000°C should be about 2 GPa. At higher pressures, it is believed that the phase assemblage Cor + CaPv should remain stable since both phases are stable up to at least the *P* at the core-mantle boundary of the Earth. It follows that this portion of our phase diagram fully supports the results of *Mao et al.* [1977] (1000–1200°C, 29.7 and 40 GPa) and *Takafuji et al.* [2002] (~800–1000°C, 23–25 GPa), but disagrees with the results of *Liu* [1979] (1000°C, 25–28 GPa), *Yusa et al.* [1995] (~1000–1500°C, ~30 GPa), and *Gréaux et al.* [2011b] (~800–1000°C, 23–25 GPa). The *P* values in *Liu* [1979] were empirically estimated by using the length of the spring used on the DAC, so that they might have been substantially overestimated, as pointed out by *Liu et al.* [2006]; if this is true, then the experiments in *Liu* [1979] were still in the stability field of Gr, which might have had a slightly distorted structure due to the deviatoric stress in the DAC. For the DAC experiments with the Gr starting material done by *Yusa et al.* [1995], the heating duration might be too short for triggering the breakdown reaction. As to the MA experiments done by *Gréaux et al.* [2011b], slow reaction rate caused by low experimental *T* and short heating duration (in situ synchrotron experiments using Gr as starting material) are the possible explanations. In *Gréaux et al.* [2011b, Figure 6] there is a phase transition curve between Gr and Gr + CaPv [P(GPa) = $-0.0082 \times T$(K) + 33.05; $T < \sim$1300 K], which is highly unlikely problem-free; with the achievement of full chemical equilibrium, Gr cannot be stable on both sides of such a phase boundary.

[48] At higher temperatures, taking 1600°C as an example, Figure 9 suggests that Gr also breaks down to Cor + CaPv [univariant reaction (St)], which is in sharp contrast to the breakdown product of CaPv + CAS as observed in *Gréaux et al.* [2011b]. From the consideration of mass balance, the breakdown of Gr to CaPv + CAS is feasible, provided that the Ca:Si molar ratio of the CaPv phase is much higher than 1 or the Ca/Si molar ratio of the CAS phase closely approaches 1. Indeed, the Ca:Si molar ratio of CaPv coexisting with no other silicate phases has the potential to be over 1 [*Fitz Gerald and Ringwood*, 1991; *Bläß et al.*, 2004; *Kojitani et al.*, 2009]. However, the compositional data of CaPv in equilibrium with other silicate phases have rarely demonstrated a Ca:Si molar ratio larger than 1 (Figure 8b). Some compositional data of CaPv reported by *Gréaux et al.* [2011b] have Ca:Si molar ratio marginally larger than 1, which might be explained by the uncertainty in the analyses, as pointed out by the authors. Alternatively, this slightly larger Ca:Si molar ratio probably actually indicates a relatively poor equilibrium state; as experimental *T* and/or heating duration increases, it slowly diminishes [*Takafuji et al.*, 2002; *Gréaux et al.*, 2011b]. On the other hand, the Ca/Si molar ratio of the CAS phase, reported so far [*Irifune et al.*, 1994; *Gautron et al.*, 1996; *Hirose and Fei*, 2002; *Zhai and Ito*, 2008], appears seldom exceeding 0.5; the only case with a Ca/Si molar ratio larger than 0.5 was reported by *Gréaux et al.* [2011b] (0.55), but that experiment (S2152) was held at 1427°C for only a few minutes, and the phase composition might have not reached its equilibrium. It appears that the breakdown of Gr to CaPv + CAS, as observed by *Gréaux et al.* [2011b], is highly unlikely. As to the existence of CAS in many experiments in *Gréaux et al.* [2011b], we must resort to their starting compositions, which indeed were richer in SiO_2, by about 0.75 wt%, than the ideal Gr composition. What had happened in the high-*T* experiments (at 1727°C for example) in *Gréaux et al.* [2011b], therefore, was that Gr + St(minor) first changed at a relatively low *P* to the phase assemblage CAS (minor) + CaPv(minor) + Gr [the univariant reaction (Cor) shown in Figure 9], then changed at a relatively high *P* to the phase assemblage CaPv + Cor(minor) + CAS [the univariant reaction (St) shown in Figure 9]. If one treated the phase assemblage CAS(minor) + CaPv(minor) + Gr as something along the Gr-breakdown curve, and missed the minor Cor in

Table 3. Parameters of Equations of State Used for the Density-Pressure Profile Calculation

Phase[a]	ρ_0 (Å^3)	$K_{300,0}$ (GPa)	$\partial K_{T,0}/\partial T$ (GPa/K)	$K'_{300,0}$	a $\times 10^{-5}$ (K^{-1})	b $\times 10^{-9}$ (K^{-2})	c (K)
Ab	2.62	57.7	−0.027[b]	4[c]	3.12	0	0
An	2.76	81.5	−0.027[b]	4[c]	1.11	0	0
CaPv	4.2	232	−0.033	4.8	3.10	0	0
CAS	3.89	171	−0.023	5.1	3.09	0	0
CF	3.88	220	−0.027[b]	4.1	3.21[d]	2.30[d]	2.24[d]
Coe	2.92	97.4	−0.027[b]	4.3	1.02	−0.45	0
Cor	3.98	258	−0.020	4.88	2.6	1.81	−0.67
Gr	3.60	166	−0.019	4[c]	2.62	0	0
Holl-I	3.89	183	−0.033	4[c]	3.32	10.9	0
Holl-II	3.98	232	−0.045[e]	4[c]	3.32[e]	10.9[e]	0[e]
Jd	3.34	125	−0.017	5.0[c]	2.56	2.60	0
Ky	3.68	192	−0.027[b]	6	2.03	10.1	0
Qtz	2.65	37.12	−0.027[b]	5.99	1.42	0.97	−1.70
San	2.55	54.1	−0.027[b]	4[c]	1.93	0	0
St	4.29	296	−0.046	4.2	1.26	12.9	0
Wd	3.08	97	−0.027[b]	4[c]	2.47	2.47	0

[a]All phases assumed to be pure end-members. Data source: Ab, *Angel et al.* [1988] and *Hovis et al.* [1999]; An, *Angel et al.* [1988] and *Czank and Schulz* [1971]; CaPv, *Wang et al.* [1996]; CAS, *Gréaux et al.* [2011a]; CF, *Dubrovinsky et al.* [2002]; Coe, *Angel et al.* [2001] and *Bourova et al.* [2006]; Cor, *Dubrovinsky et al.* [1998]; Gr, *Gréaux et al.* [2011c]; Holl-I, *Nishiyama et al.* [2005]; Holl-II, *Hirao et al.* [2008]; Jd, *Zhao et al.* [1997]; Ky, *Liu et al.* [2009, 2010b]; Qtz, *Fei* [1995] and *Angel et al.* [1997]; San, *Angel et al.* [1988] and *Hovis et al.* [1999]; St, *Nishiyama et al.* [2005]; Wd, (Chang, L. et al., Expansivity and compressibility of wadeite-type $K_2Si_4O_9$ determined by in situ high T/P experiments, and their implication, submitted to *Phys. Chem. Miner*, 2012).

[b]Assumed value which is the average of those of CaPv, CAS, Cor, Gr, Holl-I, Jd, and St.

[c]Fixed value.

[d]Same value as $CaFe_2O_4$ calcium ferrite by *Skinner* [1966].

[e]Value estimated so that there is no apparent density discontinuity along the second-order phase transition of Holl-I to Holl-II [*Sueda et al.*, 2004; *Nishiyama et al.*, 2005; *Ferroir et al.*, 2006].

the phase assemblage CaPv + Cor(minor) + CAS, a phase diagram shown as in Figure 6 in *Gréaux et al.* [2011b] should have been derived indeed.

9. Density-Pressure Profiles of the An and Gr Compositions and Their Geophysical Significance

[49] We used the third-order high-T Birch-Murnaghan equation of state to calculate the density profiles of the An and Gr compositions along the geotherms of cold slab, hot slab and normal mantle (equations (20)–(24)):

$$P=\frac{3}{2}K_{T,0}\left[\left(\frac{\rho(T,P)}{\rho(T,0)}\right)^{\frac{7}{3}}-\left(\frac{\rho(T,P)}{\rho(T,0)}\right)^{\frac{5}{3}}\right]\times\left\{1-\frac{3}{4}\left(4-K'_{T,0}\right)\left[\left(\frac{\rho(T,P)}{\rho(T,0)}\right)^{2/3}-1\right]\right\}, \quad (20)$$

$$K_{T,0}=K_{300,0}+\left(\frac{\partial K_{T,0}}{\partial T}\right)_P(T-300), \quad (21)$$

$$\rho(T,0)=\rho_0/\exp\int_{300}^{T}\alpha_{T,0}dT, \quad (22)$$

$$K'_{T,0}=K'_{300,0}, \quad (23)$$

and

$$\alpha_{T,0}=a+bT+c/T^2, \quad (24)$$

where $K_{T,0}$, $K'_{T,0}$, $\rho(T, 0)$, and $\alpha_{T,0}$ are the isothermal bulk modulus, its pressure derivative, density, and thermal expansivity of individual phase at T and ambient P, respectively. In addition, we similarly calculated the density-pressure profiles of the Ab, Or and Qtz compositions. The parameters of the equations of state for all the relevant phases used in the calculations are summarized in Table 3.

[50] As to the An composition, the sequences of the phase assemblages (Figures 3 and 9) are

$$\begin{aligned}An &\xrightarrow{\sim 2GPa} \frac{1}{3}Gr+\frac{2}{3}Ky+\frac{1}{3}Qtz \xrightarrow{\sim 2.5GPa} \frac{1}{3}Gr+\frac{2}{3}Ky\\ &+\frac{1}{3}Coe \xrightarrow{\sim 7.5GPa} \frac{1}{3}Gr+\frac{2}{3}Ky+\frac{1}{3}St \xrightarrow{\sim 14.5GPa} \frac{1}{3}Gr\\ &+\frac{2}{3}Cor+St \xrightarrow{\sim 21.5GPa} St+Cor+CaPv, \end{aligned} \quad (25)$$

$$\begin{aligned}An &\xrightarrow{\sim 2GPa} \frac{1}{3}Gr+\frac{2}{3}Ky+\frac{1}{3}Qtz \xrightarrow{\sim 3GPa} \frac{1}{3}Gr+\frac{2}{3}Ky\\ &+\frac{1}{3}Coe \xrightarrow{\sim 8GPa} \frac{1}{3}Gr+\frac{2}{3}Ky+\frac{1}{3}St \xrightarrow{\sim 143.5GPa} \frac{1}{3}Gr\\ &+\frac{2}{3}Cor+St \xrightarrow{\sim 20.5GPa} \frac{1}{5}Gr+\frac{2}{5}CAS\\ &+\frac{3}{5}St \xrightarrow{\sim 21.5GPa} \frac{1}{2}CAS+\frac{1}{2}CaPv+\frac{1}{2}St \xrightarrow{\sim 22.5GPa} St\\ &+Cor+CaPv, \end{aligned} \quad (26)$$

and

$$\begin{aligned}An &\xrightarrow{\sim 3GPa} \frac{1}{3}Gr+\frac{2}{3}Ky+\frac{1}{3}Coe \xrightarrow{\sim 9.5GPa} \frac{1}{3}Gr+\frac{2}{3}Ky\\ &+\frac{1}{3}St \xrightarrow{\sim 14.5GPa} \frac{1}{5}Gr+\frac{2}{5}CAS+\frac{3}{5}St \xrightarrow{\sim 20.5GPa} \frac{1}{2}CAS\\ &+\frac{1}{2}CaPv+\frac{1}{2}St \xrightarrow{\sim 26.5GPa} St+Cor+CaPv \end{aligned} \quad (27)$$

for the P-T conditions of the cold slab, hot slab and normal mantle, respectively [*Thompson*, 1992; *Jackson*, 1998]. As to the Gr composition, on the other hand, the sequences of the phase assemblages for the P-T conditions of the cold

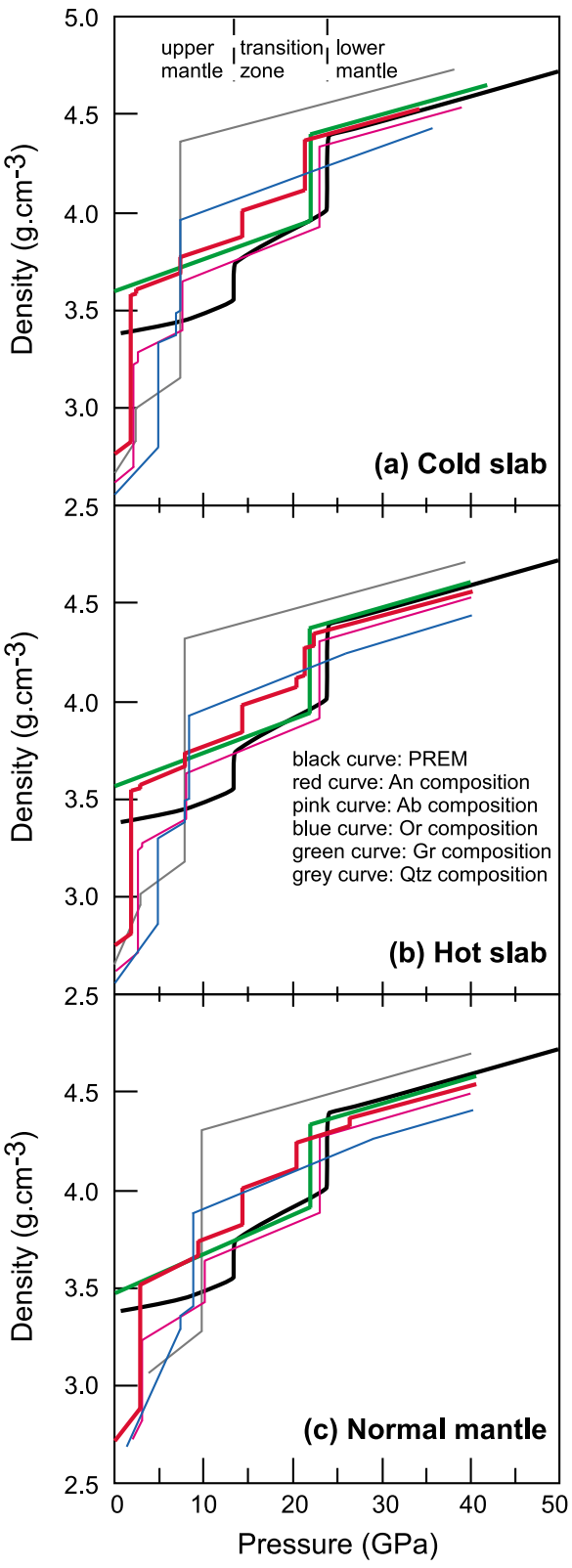

slab, hot slab and normal mantle are generally identical (Figure 9):

$$Gr \xrightarrow{\sim 21.5 GPa} Cor + 3CaPv. \quad (28)$$

It must be emphasized that inevitable uncertainty is present in these phase assemblage sequences along the geotherms of the cold slab and hot slab. The phase relations of the An and Gr compositions at very low temperatures such as 600°C have not been experimentally explored yet.

[51] The calculated density-pressure profiles, compared to the PREM density profile [*Dziewonski and Anderson*, 1981], are shown in Figure 10. As the temperature increases from the geotherm of the cold slab, through that of the hot slab, to that of the normal mantle, the density-pressure profile of every investigated composition shifts slightly to lower density, but the major features of the density-pressure profile do not change significantly.

[52] For the Qtz composition, the density of the phase assemblage of Qtz or Coe is lower than the mantle material (pyrolite) [*Ringwood*, 1966]. With the phase transition from Coe to St, the density increases significantly, and becomes substantially larger than the mantle material by ~0.9 g/cm^3 for the P interval of ~9 to 13 GPa, by ~0.6 g/cm^3 for the mantle transition zone and by ~0.1 g/cm^3 for the lower mantle.

[53] For the Gr composition, the density of the phase assemblage of Gr is larger than the upper mantle material by ~0.25 g/cm^3, but generally identical to the mantle material in the mantle transition zone. The breakdown pressure of Gr (~21.5 GPa) to Cor + 3CaPv is close to the pressure at the boundary between the mantle transition zone and lower mantle (~23 GPa), which leads to a complicated picture of the density relationship between the Gr composition and mantle material in the P interval of ~21.5–23 GPa. In the lower mantle, the density of the phase assemblage of Cor + 3CaPv is generally similar to the mantle material.

[54] For the An composition, the density of the phase assemblage of An at P less than ~2.5 GPa is much lower than the mantle material, generally by ~0.6 g/cm^3. With the breakdown of An to 1/3Gr + 2/3Ky + 1/3Qtz at ~2.5 GPa, the density of this material becomes larger than the mantle material (by ~0.2 g/cm^3). Whatever further phase transition takes place either in the An composition or in the mantle material at higher pressures, this density relationship between these two materials maintains until the pressure of ~23 GPa (Figure 10).

Figure 10. Density-pressure profiles of the An and Gr compositions at the *P-T* conditions of (a) cold slab, (b) hot slab, and (c) normal mantle. To facilitate the comparison, the density-pressure profiles of the Or, Ab and Qtz compositions are calculated and plotted, and the density-pressure profile of the PREM model are sketched as well [*Dziewonski and Anderson*, 1981]. The *P-T* data for the cold slab and hot slab are from *Thompson* [1992] while those for the normal mantle follow the 1600 K adiabat for the simplified pyrolite composition in *Jackson* [1998]. For the normal mantle *P-T* conditions, the density-pressure data for the phase assemblages of Qtz for the Qtz composition, of leucite + melt for the Or composition, of melt and Jd + Qtz for the Ab composition are ignored, which by no means affects the major conclusion drawn here.

[55] For the Ab and Or compositions, their densities remain smaller than the mantle material in the *P* interval from 0 to ~7.5–10 GPa, where the reactions of Coe→St (mainly in the Ab composition) and Wad + Ky + Coe/St→Holl-I (in the Or composition) take place. In the *P* interval from ~7.5–10 to ~13 GPa, the density of the Ab composition becomes larger than the mantle material (by ~0.2 g/cm^3), but becomes identical to or slightly smaller than the mantle material in the mantle transition zone and lower mantle. In the *P* interval from ~7.5–10 to ~23 GPa, in contrast, the density of the Or composition is significantly larger than the mantle material (by ~0.5 g/cm^3 for the *P* interval from ~8 to ~13 GPa and ~0.2 g/cm^3 for the mantle transition zone). In the lower mantle, its density becomes smaller again.

[56] In brief, the density of the An composition is significantly larger than the mantle material in the *P* range from ~2.5 to 23 GPa, that of the Or composition larger in the *P* range of ~7.5–10 to 23 GPa, and that of the Ab composition larger in the *P* range of ~7.5–10 to 13 GPa. In addition, the density of the Gr composition is substantially larger than that of the mantle material at pressures less than ~13 GPa whereas that of the Qtz composition is larger at pressures higher than ~9 GPa.

[57] Consequently, the proportion of the constituent phases of the continental crust material should have strong influence on the geophysical behavior of this material: if the continental crust material is extremely enriched in the An component, the "depth of no return" for the subducted continental crust should then be close to 2.5 GPa rather than ~7.5–10 GPa; but if it is enriched in the components of Qtz, Or and Ab, the "depth of no return" for the subducted continental crust should be ~7.5–10 GPa, as experimentally demonstrated by *Irifune et al.* [1994] and *Wu et al.* [2009]. In the *P* interval from ~2.5 to ~7.5–10 GPa, the difference in the densities of the Or, Ab, An and Qtz compositions is as large as ~0.9 g/cm^3, so that there could be a very steep density-pressure profile for the subducted continental material if the low melting components such as Or, Ab and Qtz are gradually removed by a continuous melting process as the material is being subducted down. In the *P* interval between ~7.5–10 to ~23 GPa, all the compositions of Or, Ab, An and Qtz, with the only exception of Ab at pressures from ~13 to 23 GPa (less dense by ~0.1 g/cm^3), are much more dense than the mantle material, so that the continental crust material should cascade into the deep interior of the upper mantle. In addition, it is also possible for the continental crust material to have a steep density-pressure profile since the density difference among the compositions of Or, Ab, An and Qtz is as large as ~0.6 g/cm^3, which might partially explain the high density gradient of the mantle transition zone. At pressures higher than ~23 GPa the composition of Qtz is the only one left which has a density larger than the surrounding mantle material, so that the continental crust material should have little chance to penetrate the boundary between the mantle transition zone and lower mantle of the Earth.

[58] The continental crust is mainly made of ~60% feldspar, ~15% quartz and ~15% pyroxene [*Taylor and McLennan*, 1985; *Rudnick and Fountain*, 1995]. Since pyroxene occurs both in the continental crustal material and mantle material, its influence on the density relationship of these two materials at high *P* should be generally minor. The calculated density profiles of the compositions of Or, Ab, An and Qtz therefore supply important constraints to the subduction process of the continental crust material. Compared to the surrounding mantle, the subducted continental crust material is relatively buoyant at depths shallower than ~80–250 km, the exact depth being subject to the bulk composition of the subducted crust material and the modification of the bulk composition during the subduction process. At greater depths up to the mantle transition zone-lower mantle boundary of the Earth, the buoyancy force does not exist anymore, so that the subducted continental crust material will never be positively exhumed to the Earth's surface, but contained and digested in the mantle transition zone.

10. Conclusion

[59] By performing the high-*P* MA experiments with the An composition, we have reached the following conclusions:

[60] 1. The CAS phase is a complex solid solution with multiple cation substitution mechanisms. In the CAS system, the dominant substitution mechanism is $3Si^{4+} = 4Al^{3+}$; in the CMAS system, the substitution mechanisms $Si^{4+} + Mg^{2+} = 2Al^{3+}$ and $Si^{4+} + Ca^{2+} = 2Al^{3+}$ operate; in the CAS-Na system, the substitution mechanism $Si^{4+} + Na^{+} = Al^{3+} + Ca^{2+}$ takes place [*Akaogi et al.*, 2010]. For the CAS phase in the natural rock compositions, the leading substitution mechanisms are $Si^{4+} + Mg^{2+} = 2Al^{3+}$ and $Si^{4+} + Ca^{2+} = 2Al^{3+}$.

[61] 2. The CaPv coexisting with other silicate phases has a low Al_{pfu}, usually less than 0.2. The dominant substitution mechanism is $Si^{4+} = Al^{3+} + 0.5O_v^{2+}$, rather than $Si^{4+} + Ca^{2+} = 2Al^{3+}$.

[62] 3. The subsolidus *P-T* phase diagram of the An composition has been completed up to ~25 GPa. Combining it with the results from other studies of other compositions and following the method of Schreinemakers, a *P-T* phase diagram has been obtained for a portion of the CAS system.

[63] 4. Melting of the An composition has been less well constrained. At ~14 GPa, partial melting of the phase assemblages Gr + Ky + St and Gr + CAS + St [*Gautron et al.*, 1996] is peritectic, with St as the first phase to melt out. At ~22 GPa, partial melting of the phase assemblage CaPv + CAS + St is eutectic, with St as the first phase to melt out as well. Melts at both pressures are generally andesitic.

[64] 5. The Gr composition at high *P-T* condition has a relatively simple phase diagram; Gr is stable up to ~21.5 GPa, and then decomposes to Cor + CaPv. The discrepancies in the experimental literature can be explained by the slow cation diffusion in the Gr crystal structure and compositional deviation of the experimental starting materials from the ideal Gr composition.

[65] 6. The density of the An composition starts to be higher than that of the surrounding mantle material at ~2.5 GPa, so that some An-enriched continental crust materials might positively enter the interior of the upper mantle at much shallower depths than 250 km. The large difference in the densities of the compositions Or, Ab, An and Qtz and their potential proportion variation with depth presumably caused by gradual partial melting process might partially explain the high density gradient in the upper mantle and mantle transition zone. Eventually the subducted continental crust material will be homogenized by the mantle material along the mantle transition zone-lower mantle boundary of the Earth.

[66] **Acknowledgments.** We thank T. Inoue, S. Sakamoto, Y. Higo, Y. Sueda, T. Shinmei, and D. Yamazaki for technique support. We thank Y. Fei, Y. Zhang, B. Li and L. Zhang for stimulating scientific discussions. Reviews by S. Keshav and one anonymous reviewer significantly improved the quality of the manuscript. Editor M. Walter also provided important comments on the manuscript. This work was carried out with a postdoctoral fellowship of the Japan Society for the Promotion of Science to X.L. During preparation of the manuscript, X.L. received financial support from the National Natural Science Foundation of China (grant 41090371).

References

Ahmed-Zaïd, I., and M. Madon (1995), Electron microscopy of high-pressure phases synthesized from natural garnets in a diamond anvil cell: Implications for the mineralogy of the lower mantle, *Earth Planet. Sci. Lett.*, *129*, 233–247, doi:10.1016/0012-821X(94)00245-T.

Akaogi, M., N. Kamii, A. Kishi, and H. Kojitani (2004a), Calorimetric study on high pressure transitions in $KAlSi_3O_8$, *Phys. Chem. Miner.*, *31*, 85–91, doi:10.1007/s00269-003-0372-9.

Akaogi, M., M. Yano, Y. Tejima, and H. Hojitani (2004b), High-pressure transitions of diopside and wollastonite: Phase equilibria and thermochemistry of $CaMgSi_2O_6$, $CaSiO_3$ and $CaSi_2O_5$-$CaTiSiO_5$ system, *Phys. Earth Planet. Inter.*, *143–144*, 145–156, doi:10.1016/j.pepi.2003.08.008.

Akaogi, M., M. Haraguchi, M. Yaguchi, and H. Kojitani (2009), High-pressure phase relations and thermodynamic properties of $CaAl_4Si_2O_{11}$ CAS phase, *Phys. Earth Planet. Inter.*, *173*, 1–6, doi:10.1016/j.pepi.2008.10.010.

Akaogi, M., M. Haraguchi, K. Nakanishi, H. Ajiro, and H. Kojitani (2010), High-pressure phase relations in the system $CaAl_4Si_2O_{11}$-$NaAl_3Si_3O_{11}$ with implication for Na-rich CAS phase in shocked Martian meteorites, *Earth Planet. Sci. Lett.*, *289*, 503–508, doi:10.1016/j.epsl.2009.11.043.

Andrault, D., G. Fiquet, F. Guyot, and M. Hanfland (1998), Pressure-induced Landau-type transition in stishovite, *Science*, *282*, 720–724, doi:10.1126/science.282.5389.720.

Andrault, D., R. J. Angel, J. L. Mosenfelder, and T. Le Bihan (2003), Equation of state of stishovite to lower mantle pressures, *Am. Mineral.*, *88*, 301–307.

Angel, R. J., R. M. Hazen, T. C. McCormick, C. T. Prewitt, and J. R. Smyth (1988), Comparative compressibility of end-member feldspars, *Phys. Chem. Miner.*, *15*, 313–318, doi:10.1007/BF00311034.

Angel, R. J., D. R. Allan, R. Miletich, and L. W. Finger (1997), The use of quartz as an internal pressure standard in high-pressure crystallography, *J. Appl. Crystallogr.*, *30*, 461–466, doi:10.1107/S0021889897000861.

Angel, R. J., J. L. Mosenfelder, and C. S. J. Shaw (2001), Anomalous compression and equation of state of coesite, *Phys. Earth Planet. Inter.*, *124*, 71–79, doi:10.1016/S0031-9201(01)00184-4.

Asahara, Y., E. Ohtani, T. Kondo, T. Kubo, N. Miyajima, T. Nagase, K. Fujino, T. Yagi, and T. Kikegawa (2005), Formation of metastable cubic-perovskite in high-pressure phase transformation of Ca(Mg, Fe, Al)Si_2O_6, *Am. Mineral.*, *90*, 457–462, doi:10.2138/am.2005.1649.

Beck, P., P. Gillet, L. Gautron, I. Daniel, and A. El Goresy (2004), A new natural high-pressure (Na,Ca)-hexaluminosilicate [$(Ca_xNa_{1-x})Al_{3+x}Si_{3-x}O_{11}$] in shocked Martian meteorites, *Earth Planet. Sci. Lett.*, *219*, 1–12, doi:10.1016/S0012-821X(03)00695-2.

Bertka, C. M., and Y. Fei (1997), Mineralogy of Martian interior up to core-mantle boundary pressures, *J. Geophys. Res.*, *102*, 5251–5264, doi:10.1029/96JB03270.

Birch, F., and P. LeComte (1960), Temperature-pressure plane for albite composition, *Am. J. Sci.*, *258*, 209–217, doi:10.2475/ajs.258.3.209.

Bläß, U. W., F. Langenhorst, T. Boffa-Ballaran, F. Seifert, D. J. Frost, and C. A. McCammon (2004), A new oxygen-deficient perovskite phase Ca$(Fe_{0.4}Si_{0.6})O_{2.8}$ and phase relations along the join $CaSiO_3$-$CaFeO_{2.5}$ at transition zone conditions, *Phys. Chem. Miner.*, *31*, 52–65, doi:10.1007/s00269-003-0375-6.

Bourova, E., P. Richet, and J. P. Petitet (2006), Coesite (SiO_2) as an extreme case of superheated crystal: An X-ray diffraction study up to 1776 K, *Chem. Geol.*, *229*, 57–63, doi:10.1016/j.chemgeo.2006.01.011.

Boyd, F. R., and J. L. England (1961), Melting of silicates at high pressures, *Year Book Carnegie Inst. Washington*, *60*, 113–125.

Czank, M., and H. Schulz (1971), Thermal expansion of anorthite, *Naturwissenschaften*, *58*, 94, doi:10.1007/BF00595022.

Deng, L., X. Liu, H. Liu, and J. Dong (2010), High-pressure phase relations in the composition of albite $NaAlSi_3O_8$ constrained by an ab initio and quasi-harmonic Debye model, and their implications, *Earth Planet. Sci. Lett.*, *298*, 427–433, doi:10.1016/j.epsl.2010.08.008.

Deng, L., X. Liu, H. Liu, and Y. Zhang (2011), A first-principles study of the phase transition from Holl-I to Holl-II in the composition $KAlSi_3O_8$, *Am. Mineral.*, *96*, 974–982, doi:10.2138/am.2011.3689.

Dubrovinsky, L. S., S. K. Saxena, P. Lazor, R. Ahuja, O. Eriksson, J. M. Wills, and B. Johansson (1997), Experimental and theoretical identification of a new high-pressure phase of silica, *Nature*, *388*, 362–365, doi:10.1038/41066.

Dubrovinsky, L. S., S. K. Saxena, and P. Lazor (1998), High-pressure and high-temperature in situ X-ray diffraction study of iron and corundum to 68 GPa using an internally heated diamond anvil cell, *Phys. Chem. Miner.*, *25*, 434–441, doi:10.1007/s002690050133.

Dubrovinsky, L. S., N. A. Dubrovinskaia, V. B. Prokopenko, and T. Le Bihan (2002), Equation of state and crystal structure of NaAlSiO_4 with calcium-ferrite type structure in the conditions of the lower mantle, *High Pressure Res.*, *22*, 495–499, doi:10.1080/08957950212807.

Dupré, B., and C. J. Allègre (1983), Pb-Sr isotope variation in Indian ocean basalts and mixing phenomena, *Nature*, *303*, 142–146, doi:10.1038/303142a0.

Dziewonski, A. M., and D. L. Anderson (1981), Preliminary reference Earth model, *Phys. Earth Planet. Inter.*, *25*, 297–356, doi:10.1016/0031-9201(81)90046-7.

Fei, Y. (1995), Thermal expansion, in *Mineral Physics and Crystallography: A Handbook of Physical Constants*, *AGU Ref. Shelf*, vol. 2, edited by T. J. Ahrens, pp. 29–44, AGU, Washington, D. C., doi:10.1029/RF002p0029.

Fei, Y., and C. M. Bertka (1999), Phase transitions in the Earth's mantle and mantle mineralogy, in *Mantle Petrology: Field Observations and High Pressure Experimentation: A Tribute to Francis R. (Joe) Boyd*, *Geochem. Soc. Spec. Publ.*, vol. 6, edited by Y. Fei, C. M. Bertka, and B. O. Mysen, pp. 189–207, Geochem. Soc., Houston, Tex.

Ferroir, T., T. Onozawa, T. Yagi, S. Merkel, N. Miyajima, N. Nishiyama, T. Irifune, and T. Kikegawa (2006), Equation of state and phase transition in $KAlSi_3O_8$ hollandite at high pressure, *Am. Mineral.*, *91*, 327–332, doi:10.2138/am.2006.1879.

Fitz Gerald, J. D., and A. E. Ringwood (1991), High pressure rhombohedral perovskite phase $Ca_2AlSiO_{5.5}$, *Phys. Chem. Miner.*, *18*, 40–46, doi:10.1007/BF00199042.

Funamori, N., and R. Jeanloz (1997), High-pressure transformation of Al_2O_3, *Science*, *278*, 1109–1111, doi:10.1126/science.278.5340.1109.

Funamori, N., R. Jeanloz, N. Miyajima, and K. Fujino (2000), Mineral assemblages of basalt in the lower mantle, *J. Geophys. Res.*, *105*, 26,037–26,043, doi:10.1029/2000JB900252.

Gautron, L., and M. Madon (1994), A study of the stability of anorthite in the PT conditions of Earth's transition zone, *Earth Planet. Sci. Lett.*, *125*, 281–291, doi:10.1016/0012-821X(94)90221-6.

Gautron, L., S. E. Kesson, and W. O. Hibberson (1996), Phase relations for $CaAl_2Si_2O_8$ (anorthite composition) in the system CaO-Al_2O_3-SiO_2 at 14 GPa, *Phys. Earth Planet. Inter.*, *97*, 71–81, doi:10.1016/0031-9201(96)03161-5.

Gautron, L., J. D. Fitz Gerald, S. E. Kesson, R. A. Eggleton, and T. Irifune (1997), Hexagonal Ba-ferrite: A good model for the crystal structure of a new high-pressure phase $CaAl_4Si_2O_{11}$?, *Phys. Earth Planet. Inter.*, *102*, 223–229, doi:10.1016/S0031-9201(97)00007-1.

Gautron, L., R. J. Angel, and R. Miletich (1999), Structural characterization of the high-pressure phase $CaAl_4Si_2O_{11}$, *Phys. Chem. Miner.*, *27*, 47–51, doi:10.1007/s002690050239.

Goldsmith, J. R. (1980), The melting and breakdown reactions of anorthite at high pressures and temperatures, *Am. Mineral.*, *65*, 272–284.

Grassi, D., and M. W. Schmidt (2011), The melting of carbonated pelites from 70 to 700 km depth, *J. Petrol.*, *52*, 765–789, doi:10.1093/petrology/egr002.

Gréaux, S., N. Nishiyama, Y. Kono, T. Irifune, and L. Gautron (2011a), P-V-T equation of state of $CaAl_4Si_2O_{11}$ CAS phase, *Phys. Chem. Miner.*, *38*, 581–590, doi:10.1007/s00269-011-0430-7.

Gréaux, S., N. Nishiyama, Y. Kono, L. Gautron, H. Ohfuji, T. Kunimoto, N. Menguy, and T. Irifune (2011b), Phase transformations of $Ca_3Al_2Si_3O_{12}$ grossular garnet to the depths of the Earth's mantle transition zone, *Phys. Earth Planet. Inter.*, *185*, 89–99, doi:10.1016/j.pepi.2011.02.001.

Gréaux, S., Y. Kono, N. Nishiyama, T. Kunimoto, K. Wada, and T. Irifune (2011c), P-V-T equation of state of $Ca_3Al_2Si_3O_{12}$ grossular garnet, *Phys. Chem. Miner.*, *38*, 85–94, doi:10.1007/s00269-010-0384-1.

Grey, I. E., I. C. Madsen, H. S. C. O'Neill, S. E. Kesson, and W. O. Hibberson (1999), Rietveld refinement of high-pressure $CaAl_4Si_2O_{11}$ with the R-type ferrite structure, *Neues Jahrb. Mineral. Monatsh.*, *3*, 104–112.

Hariya, Y., and G. C. Kennedy (1968), Equilibrium study of anorthite under high pressure and high temperature, *Am. J. Sci.*, *266*, 193–203, doi:10.2475/ajs.266.3.193.

Hays, J. F. (1966), Lime-alumina-silica, *Carnegie Inst. Washington Year Book*, *65*, 234–239.

Hirao, N., E. Ohtani, T. Kondo, T. Sakai, and T. Kikegawa (2008), Hollandite II phase in $KAlSi_3O_8$ as a potential host mineral of potassium in the Earth's lower mantle, *Phys. Earth Planet. Inter.*, *166*, 97–104, doi:10.1016/j.pepi.2007.11.002.

Hirose, K., and Y. Fei (2002), Subsolidus and melting phase relations of basaltic composition in the uppermost lower mantle, *Geochim. Cosmochim. Acta*, *66*, 2099–2108, doi:10.1016/S0016-7037(02)00847-5.

Hirose, K., N. Shimizu, W. van Westrenen, and Y. Fei (2004), Trace element partitioning in Earth's lower mantle and implications for geochemical consequences of partial melting at the core-mantle boundary, *Phys. Earth Planet. Inter.*, *146*, 249–260, doi:10.1016/j.pepi.2002.11.001.

Hirose, K., N. Takafuji, N. Sata, and Y. Ohishi (2005), Phase transition and density of subducted MORB crust in the lower mantle, *Earth Planet. Sci. Lett.*, *237*, 239–251, doi:10.1016/j.epsl.2005.06.035.

Hofmann, A. W. (1997), Mantle geochemistry: The message from oceanic volcanism, *Nature*, *385*, 219–229, doi:10.1038/385219a0.

Holland, T. J. B. (1980), The reaction albite = jadeite + quartz determined experimentally in the range 600–1200°C, *Am. Mineral.*, *65*, 129–134.

Hovis, G. L., S. Brennan, M. Keohane, and J. Crelling (1999), High-temperature X-ray investigation of sanidine-analbite crystalline solutions: Thermal expansion, phase transitions, and volume of mixing, *Can. Mineral.*, *37*, 701–709.

Irifune, T. (1994), Absence of an aluminous phase in the upper part of the Earth's lower mantle, *Nature*, *370*, 131–133, doi:10.1038/370131a0.

Irifune, T., and A. E. Ringwood (1993), Phase transformation in subducted oceanic crust and buoyancy relationships at depths of 600–800 km in the mantle, *Earth Planet. Sci. Lett.*, *117*, 101–110, doi:10.1016/0012-821X(93)90120-X.

Irifune, T., A. E. Ringwood, and W. O. Hibberson (1994), Subduction of continental crust and terrigenous and pelagic sediments: An experimental study, *Earth Planet. Sci. Lett.*, *126*, 351–368, doi:10.1016/0012-821X(94)90117-1.

Irifune, T., K. Kuroda, T. Minagawa, and M. Unemoto (1995), Experimental study of the decomposition of kyanite at high pressure and high temperature, in *The Earth's Central Part: Its Structure and Dynamics*, edited by T. Yukutake, pp. 35–44, Terra Sci., Tokyo.

Irifune, T., M. Miyashita, T. Inoue, J. Ando, K. Funakoshi, and W. Utsumi (2000), High-pressure phase transformation in $CaMgSi_2O_6$ and implications for origin of ultra-deep diamond inclusions, *Geophys. Res. Lett.*, *27*, 3541–3544, doi:10.1029/2000GL012105.

Ishibashi, K., K. Hirose, N. Sata, and Y. Ohishi (2008), Dissociation of CAS phase in the uppermost lower mantle, *Phys. Chem. Miner.*, *35*, 197–200, doi:10.1007/s00269-007-0212-4.

Ito, E., and E. Takahashi (1989), Postspinel transformations in the system Mg_2SiO_4-Fe_2SiO_4 and some geophysical implications, *J. Geophys. Res.*, *94*, 10,637–10,646, doi:10.1029/JB094iB08p10637.

Jackson, I. (1998), Elasticity, composition and temperature of the Earth's lower mantle: A reappraisal, *Geophys. J. Int.*, *134*, 291–311, doi:10.1046/j.1365-246x.1998.00560.x.

Keshav, S., and G. H. Gudfinnsson (2010), Experimentally dictated stability of carbonated oceanic crust to moderately great depths in the Earth: Results from the solidus determination in the system CaO-MgO-Al_2O_3-SiO_2-CO_2, *J. Geophys. Res.*, *115*, B05205, doi:10.1029/2009JB006457.

Kesson, S. E., J. D. Fitz Gerald, and J. M. G. Shelley (1994), Mineral chemistry and density of subducted basaltic crust at lower-mantle pressures, *Nature*, *372*, 767–769, doi:10.1038/372767a0.

Kesson, S. E., J. D. Fitz Gerald, and J. M. Shelley (1998), Mineralogy and dynamics of a pyrolite lower mantle, *Nature*, *393*, 252–255, doi:10.1038/30466.

Kingma, K. J., R. E. Cohen, R. J. Hemley, and H.-K. Mao (1995), Transformation of stishovite to a denser phase at lower mantle pressures, *Nature*, *374*, 243–245, doi:10.1038/374243a0.

Kinomura, N., S. Kume, and M. Koizumi (1975), Stability of $K_2Si_4O_9$ with wadeite type structure, in *Proceedings of the 4th International Conference on High Pressure, Kyoto, 1974*, edited by J. Osugi, pp. 211–214, Phys. Chem. Soc. of Jpn., Kyoto, Japan.

Kojitani, H., Y. Wakabayashi, Y. Tejima, C. Kato, M. Haraguchi, and M. Akaogi (2009), High-pressure phase relations in $Ca_2AlSiO_{5.5}$ and energetics of perovskite-related compounds with oxygen defects in the $Ca_2Si_2O_6$-$Ca_2Al_2O_5$ join, *Phys. Earth Planet. Inter.*, *173*, 349–353, doi:10.1016/j.pepi.2009.02.001.

Korzhinskii, D. S. (1959), *Physicochemical Basis of the Analysis of the Paragenesis of Minerals*, Consult. Bur., New York.

Lesher, C. E., and D. Walker (1988), Cumulate maturation and melt migration in a temperature gradient, *J. Geophys. Res.*, *93*, 10,295–10,311, doi:10.1029/JB093iB09p10295.

Litasov, K., and E. Ohtani (2003), Stability of various hydrous phases in CMAS pyrolite-H_2O system up to 25 GPa, *Phys. Chem. Miner.*, *30*, 147–156, doi:10.1007/s00269-003-0301-y.

Litasov, K., and E. Ohtani (2010), The solidus of carbonated eclogite in the system CaO-Al_2O_3-MgO-SiO_2-Na_2O-CO_2 to 32 GPa and carbonatite liquid in the deep mantle, *Earth Planet. Sci. Lett.*, *295*, 115–126, doi:10.1016/j.epsl.2010.03.030.

Liu, L. (1974), Disproportionation of kyanite to corundum plus stishovite at high pressure and high temperature, *Earth Planet. Sci. Lett.*, *24*, 224–228, doi:10.1016/0012-821X(74)90100-9.

Liu, L. (1978), High-pressure phase transformations of albite, jadeite and nepheline, *Earth Planet. Sci. Lett.*, *37*, 438–444, doi:10.1016/0012-821X(78)90059-6.

Liu, L. (1979), High-pressure phase transformations in the system $CaSiO_3$-Al_2O_3, *Earth Planet. Sci. Lett.*, *43*, 331–335, doi:10.1016/0012-821X(79)90219-X.

Liu, L. (1987), High-pressure phase transitions of potassium aluminosilicates with an emphasis on leucite, *Contrib. Mineral. Petrol.*, *95*, 1–3, doi:10.1007/BF00518025.

Liu, L., and A. E. Ringwood (1975), Synthesis of a perovskite-type polymorph of $CaSiO_3$, *Earth Planet. Sci. Lett.*, *28*, 209–211, doi:10.1016/0012-821X(75)90229-0.

Liu, X. (2006), Phase relations in the system $KAlSi_3O_8$-$NaAlSi_3O_8$ at high pressure-high temperature conditions and their implication to the petrogenesis of lingunite, *Earth Planet. Sci. Lett.*, *246*, 317–325, doi:10.1016/j.epsl.2006.04.016.

Liu, X., N. Nishiyama, T. Sanehira, T. Inoue, Y. Higo, and S. Sakamoto (2006), Decomposition of kyanite and solubility of Al_2O_3 in stishovite at high pressure and high temperature conditions, *Phys. Chem. Miner.*, *33*, 711–721, doi:10.1007/s00269-006-0122-x.

Liu, X., S. R. Shieh, M. E. Fleet, and L. Zhang (2009), Compressibility of a natural kyanite to 17.5 GPa, *Prog. Nat. Sci.*, *19*, 1281–1286, doi:10.1016/j.pnsc.2009.04.001.

Liu, X., Z. Hu, and L. Deng (2010a), Feldspars under conditions of high temperature-high pressure, *Acta Petrol. Sin.*, *26*, 3601–3610.

Liu, X., Q. He, H. Wang, M. E. Fleet, and X. Hu (2010b), Thermal expansion of kyanite at ambient pressure: An X-ray powder diffraction study up to 1000°C, *Geosci. Front.*, *1*, 91–97, doi:10.1016/j.gsf.2010.07.002.

Liu, X., Q. He, L. Deng, S. Zhai, X. Hu, B. Li, L. Zhang, Z. Chen, and Q. Liu (2011), Equation of state of CAS phase to pressure of the uppermost lower mantle at ambient temperature, *Sci. China Earth Sci.*, *54*, 1394–1399, doi:10.1007/s11430-011-4262-6.

Madon, M., J. Castex, and J. Peyronneau (1989), A new aluminocalcic high-pressure phase as a possible host of calcium and aluminium in the lower mantle, *Nature*, *342*, 422–425, doi:10.1038/342422a0.

Mao, H. K., T. Yagi, and P. M. Bell (1977), Mineralogy of the Earth's deep mantle: Quenching experiments on mineral compositions at high pressure and temperature, *Year Book Carnegie Inst. Washington*, *76*, 502–504.

Mookherjee, M., and G. Steinle-Neumann (2009), Detecting deeply subducted crust from the elasticity of hollandite, *Earth Planet. Sci. Lett.*, *288*, 349–358, doi:10.1016/j.epsl.2009.09.037.

Nishiyama, N., and T. Yagi (2003), Phase relation and mineral chemistry in pyrolite to 2200°C under the lower mantle pressures and implications for dynamics of mantle plumes, *J. Geophys. Res.*, *108*(B5), 2255, doi:10.1029/2002JB002216.

Nishiyama, N., R. P. Rapp, T. Irifune, T. Sanehira, D. Yamazaki, and K. Funakoshi (2005), Stability and P-V-T equation of state of $KAlSi_3O_8$-hollandite determined by in situ X-ray observations and implications for dynamics of subducted continental crust material, *Phys. Chem. Miner.*, *32*, 627–637, doi:10.1007/s00269-005-0037-y.

Okamoto, K., and S. Maruyama (2004), The eclogite-garnetite transformation in the MORB + H_2O system, *Phys. Earth Planet. Inter.*, *146*, 283–296, doi:10.1016/j.pepi.2003.07.029.

Ono, S., E. Ito, and T. Katsura (2001), Mineralogy of subducted basaltic crust (MORB) from 25 to 37 GPa, and chemical heterogeneity of the lower mantle, *Earth Planet. Sci. Lett.*, *190*, 57–63, doi:10.1016/S0012-821X(01)00375-2.

Ono, S., T. Iizuka, and T. Kikegawa (2005), Compressibility of the calcium aluminosilicate, CAS, phase to 44 GPa, *Phys. Earth Planet. Inter.*, *150*, 331–338, doi:10.1016/j.pepi.2004.12.001.

Ono, S., Y. Nakajima, and K. Funakoshi (2007), In situ observation of the decomposition of kyanite at high pressures and high temperatures, *Am. Mineral.*, *92*, 1624–1629, doi:10.2138/am.2007.2492.

Presnall, D. C. (1995), Phase diagrams of Earth-Forming minerals, in *Mineral Physics and Crystallography: A Handbook of Physical Constants*, *AGU Ref. Shelf*, vol. 2, edited by T. J. Ahrens, pp. 248–268, AGU, Washington, D. C., doi:10.1029/RF002p0248.

Rapp, R. P., T. Irifune, N. Shimizu, N. Nishiyama, M. D. Norman, and T. Inoue (2008), Subduction recycling of continental sediments and the origin of geochemically enriched reservoirs in the deep mantle, *Earth Planet. Sci. Lett.*, *271*, 14–23, doi:10.1016/j.epsl.2008.02.028.

Reid, A. F., and A. E. Ringwood (1969), Six-coordinate silicon: High pressure strontium and barium aluminosilicates with the hollandite structure, *J. Solid State Chem.*, *1*, 6–9, doi:10.1016/0022-4596(69)90002-4.

Ricolleau, A., G. Fiquet, A. Addad, N. Menguy, C. Vanni, J.-P. Perrillat, I. Daniel, H. Cardon, and N. Guignot (2008), Analytical transmission

electron microscopy study of a natural MORB sample assemblage transformed at high pressure and high temperature, *Am. Mineral.*, *93*, 144–153, doi:10.2138/am.2008.2532.

Ringwood, A. E. (1966), The chemical composition and origin of the Earth, in *Advances in Earth Sciences*, edited by P. Hurly, pp. 287–356, MIT Press, Cambridge, Mass.

Ringwood, A. E., A. F. Reid, and A. D. Wadsley (1967), High-pressure $KAlSi_3O_8$, an aluminosilicate with sixfold coordination, *Acta Crystallogr.*, *23*, 1093–1095, doi:10.1107/S0365110X6700430X.

Rudnick, R. L., and D. M. Fountain (1995), Nature and composition of the continental crust: A lower crustal perspective, *Rev. Geophys.*, *33*, 267–309, doi:10.1029/95RG01302.

Schmidt, M. W., S. Poli, P. Comodi, and P. F. Zanazzi (1997), High-pressure behavior of kyanite: Decomposition of kyanite into stishovite and corundum, *Am. Mineral.*, *82*, 460–466.

Schreinemakers, F. A. H. (1915), *In-, Mono-, and Divariant Equilibria*, Muller, Amsterdam.

Skinner, B. J. (1966), Thermal expansion, in *Handbook of Physical Constants*, edited by S. P. Clark, *Mem. Geol. Soc. Am.*, 97, 75–96.

Sueda, Y., T. Irifune, N. Nishiyama, R. P. Rapp, T. Ferroir, T. Onozawa, T. Yagi, S. Merkel, N. Miyajima, and K. Funakoshi (2004), A new high-pressure form of $KAlSi_3O_8$ under lower mantle conditions, *Geophys. Res. Lett.*, *31*, L23612, doi:10.1029/2004GL021156.

Takafuji, N., T. Yagi, N. Miyajima, and T. Sumita (2002), Study on Al_2O_3 content and phase stability of aluminous-$CaSiO_3$ perovskite at high pressure and temperature, *Phys. Chem. Miner.*, *29*, 532–537, doi:10.1007/s00269-002-0271-5.

Taylor, S. R., and S. M. McLennan (1985), *The Continental Crust: Its Composition and Evolution*, Blackwell Sci, Oxford, UK.

Thompson, A. B. (1992), Water in the Earth's upper mantle, *Nature*, *358*, 295–302, doi:10.1038/358295a0.

Tutti, F., S. D. Leonid, and K. S. Surendra (2000), High pressure phase transformation of jadeite and stability of $NaAlSiO_4$ with calcium-ferrite type structure in the lower mantle conditions, *Geophys. Res. Lett.*, *27*, 2025–2028, doi:10.1029/2000GL008496.

Urakawa, S., T. Kondo, N. Igawa, O. Shimomura, and H. Ohno (1994), Synchrotron radiation study on the high-pressure and high-temperature phase relations of $KAlSi_3O_8$, *Phys. Chem. Miner.*, *21*, 387–391, doi:10.1007/BF00203296.

Walter, M. J., T. W. Sisson, and D. C. Presnall (1995), A mass proportion method for calculating melting reaction and application to melting of model upper mantle lherzolite, *Earth Planet. Sci. Lett.*, *135*, 77–90, doi:10.1016/0012-821X(95)00148-6.

Walter, M. J., A. Kubo, T. Yoshino, J. Brodholt, K. T. Koga, and Y. Ohishi (2004), Phase relations and equation-of-state of aluminous Mg-silicate perovskite and implications for Earth's lower mantle, *Earth Planet. Sci. Lett.*, *222*, 501–516, doi:10.1016/j.epsl.2004.03.014.

Walter, M. J., R. G. Trønnes, L. S. Armstrong, O. T. Lord, W. A. Caldwell, and S. M. Clark (2006), Subsolidus phase relations and perovskite compressibility in the system $MgO\text{-}AlO_{1.5}\text{-}SiO_2$ with implications for Earth's lower mantle, *Earth Planet. Sci. Lett.*, *248*, 77–89, doi:10.1016/j.epsl.2006.05.017.

Wang, Y., D. J. Weidner, and F. Guyot (1996), Thermal equation of state of $CaSiO_3$ perovskite, *J. Geophys. Res.*, *101*, 661–672, doi:10.1029/95JB03254.

Wood, B. J. (2000), Phase transformations and partitioning relations in peridotite under lower mantle conditions, *Earth Planet. Sci. Lett.*, *174*, 341–354, doi:10.1016/S0012-821X(99)00273-3.

Wu, Y., Y. Fei, Z. Jin, and X. Liu (2009), The fate of subducted upper continental crust: An experimental study, *Earth Planet. Sci. Lett.*, *282*, 275–284, doi:10.1016/j.epsl.2009.03.028.

Xue, X., S. Zhai, and M. Kanzaki (2009), Si-Al distribution in high-pressure $CaAl_4Si_2O_{11}$ phase: A ^{29}Si and ^{27}Al NMR study, *Am. Mineral.*, *94*, 1739–1742, doi:10.2138/am.2009.3348.

Yagi, A., T. Suzuki, and M. Akaogi (1994), High pressure transitions in the system $KAlSi_3O_8\text{-}NaAlSi_3O_8$, *Phys. Chem. Miner.*, *21*, 12–17, doi:10.1007/BF00205210.

Yusa, H., T. Yagi, and N. Shimobayashi (1995), A new unquenchable high-pressure polymorph of $Ca_3Al_2Si_3O_{12}$, *Phys. Earth Planet. Inter.*, *92*, 25–31, doi:10.1016/0031-9201(95)03057-4.

Zen, E. A. (1966), Construction of pressure-temperature diagrams for multicomponent systems after the method of Schreinemakers—A geometric approach, *U.S. Geol. Surv. Bull.*, *1225*, 1–56.

Zhai, S., and E. Ito (2008), Phase relations of $CaAl_4Si_2O_{11}$ at high-pressure and high-temperature with implications for subducted continental crust into the deep mantle, *Phys. Earth Planet. Inter.*, *167*, 161–167, doi:10.1016/j.pepi.2008.03.004.

Zhao, Y., R. B. Von Dreele, T. J. Shankland, D. J. Weidner, J. Zhang, Y. Wang, and T. Gasparik (1997), Thermoelastic equation of state of jadeite $NaAlSi_2O_6$: An energy-dispersive Reitveld refinement study of low symmetry and multiple phase diffraction, *Geophys. Res. Lett.*, *24*, 5–8, doi:10.1029/96GL03769.